Transport Category Wing Weight Estimation Using A Optimizing Beam-Element Structural Formulation

Timothy T. Takahashi[1] and Tyler Lemonds[2]
Arizona State University, Tempe, AZ

This paper describes the development of a wing primary structural weight estimation method based upon an optimizing beam-element formulation. For any given outer mould-line geometry, our beam-element method sizes primary structure based upon "envelope" inertial and aerodynamic loads arising from maneuvering flight and hard-landing conditions. It sizes structure cognizant of tensile yield, compression yield, compression buckling of the skins and compression buckling limitations of integrally stiffened wing covers. Using this procedure, we synthesize a "real" structure within a given outer mould line. This structure can be rendered in CAD and used for finite-element-method (FEM) verification. Because our primary structural weights are based upon physical geometry, as opposed to simple empirical and parametric equations, we capture "real world" design effects that escape lower order methods.

Nomenclature

Basic Geometry

BL	=	Butt-line (in)
FS	=	Fuselage Station (in)
WL	=	Water Line (in)
x	=	Ordinate aligned with global fuselage station reference frame
y	=	Ordinate aligned with global butt-line reference frame
y'	=	Ordinate aligned with local, wing axis semi-span reference frame

Aircraft Geometry and Load Factors

Nz	=	Load factor in the z (Water Line) direction (g's)
Sref	=	Wing Planform Area (ft^2)
W	=	Weight representing Mass at 1g (lbm)
MTOW	=	Maximum Takeoff Weight (lbm)
MLW	=	Maximum Landing Weight (lbm)
t/c	=	Thickness to Chord Ratio of Wing Section (%)
b	=	Span of Wing (tip-to-tip) (ft)
c	=	Chord of Wing (ft)
t	=	Dimensional Thickness of Wing Sections (ft)
AR	=	Aspect Ratio (span / chord)
TR	=	Taper Ratio (ratio of tip-chord to center-line chord)
$\Lambda_{c/2}$	=	Mid Chord Sweep Angle (^{o})

Structural Analysis Equations

A	=	Cross Sectional Area of Structure (in^2)
I	=	Area Moment of Inertia (in^4)
L	=	Length (in)

[1] Professor of Practice, Aerospace and Mechanical Engineering, School for Engineering of Matter, Transport & Energy, P.O. Box 876106, Tempe, AZ. Associate Fellow AIAA.
[2] M.S. Candidate, Aerospace and Mechanical Engineering, School for Engineering of Matter, Transport & Energy, P.O. Box 876106, Tempe, AZ.

P = Force (lbf)
τ = Shear (lbf)
M = Moment (lbf-ft)
T = Torque (lbf-ft)

Materials Properties
ρ = Material Density (lbm/in^3)
E = Material Elastic Modulus (lbf/in^2)
σ_{tu} = Material Ultimate Tensile Strength (lbf/in^2)
σ_{ty} = Material Tension Yield Strength (lbf/in^2)
σ_{cy} = Material Compression Yield Strength (lbf/in^2)
σ_{su} = Material Ultimate Shear Strength (lbf/in^2)

I. Introduction

AIRCRAFT conceptual design requires the engineer to balance many competeting interests. Aerodynamics, propulsion, stability & control, maneuverability, mission performance, structural feasibility and empty weight concerns must harmoniously balance to build a vehicle that meets or exceeds required mission performance. No one discipline can be ignored without peril.

During traditional conceptual design, engineers typically employ empirical methods derived from "as-built" properties of historical aircraft in order to estimate the weight of the proposed structure. These algebraic methods may be tedious to implement, but they provide a weight estimate without substantial computational effort. As a result, methods such as Raymer [1], Roskam [2], Nicolai [3], Toorenbeek [4][5] and those contained within NASA's FLOPS sizing code [6] are used in many academic and industrial aircraft design studies.

These empirical methods have significant drawbacks. First, they expect that the historical aircraft used in the regression were all optimally designed; i.e. that the basis data isn't inherently pessimistic. Second, they assume that resulting equations are a "tight fit" of the basis data; i.e that a non-Kriging metamodel accurately predicts existing aircraft weight. Third, they presume that that the statistical regression is valid for systems design in the absence of any sort of internal structural arrangment. Fourth, they do not account for "subtle" variations in internal layout (such as the location of landing gear, or wing mounted engines when considering inertial relief).

Functionally, the traditional "empirical weights" approach to design requires the detail design team to engineer a production structure to a strict, allocated weight requirement. In industry, the ability for a structural team to achieve these goals varies from project to project. The story of the Lockheed C-5 is the most famous issue of a system-level program failure resulting from a desire to meet weight targets. [7] The original C-5 wing was designed to meet the allocated weight target at the expense of a usable fatigue life. At great expense, the government re-winged the entire early C-5 production run by swapping out the original light-weight wing for a heavier, more structurally sound wing.

The alternative design procedure, where each concept configuration requires a thorough time-intensive hand-worked structural design process proves too cumbersome to use in any systematic, multi-disiciplinary-optimization (MDO) process. Even with a large team of draftsmen and analysts, only a few designs can be "fleshed out" to any degree of confidence on a typical engineering project timetable. Aircraft designers who employ this approach burden themselves with the consequences of a "point-design" aircraft; any weight shortfall will the directly and negatively impact system performance.

To better trade the nuance between proposed advanced technology transport-category aircraft concepts, we created a design tool to automate the initial structural sizing of the torque-box of an aircraft wing. From these results, we could use this method to provide a weight estimate based on a verifiable, physical, "preliminary design" quality structure.

II. Methodology

For this paper, we built an automated structural design method suitable to design the primary structure (torque box) of a generic transport category wing.

Our method is flexible enough to address wings of arbitrary outer mould line geometry lofted according to customary principles (see Figure 1). We may vary basic planform variables: wing-span (b) (tip-to-tip), wing sweep (Λ), wing taper ratio (TR) as well as more subtle configuration elements: the spanwise variation in wing thickness-to-chord ratio ($t/c(y)$), the inter-rib spacing, the location of fuel (for intertial loads), the location of engines (for inertial relief), the location of landing gear (for both inertial relief, and for applied landing loads). We can choose to employ structural materials of varying properties: elastic modulus (E), density (ρ), yield strength in tension (σ_{ty}), yield strength in compression (σ_{cy}) and ultimate strength in shear (σ_{su}).

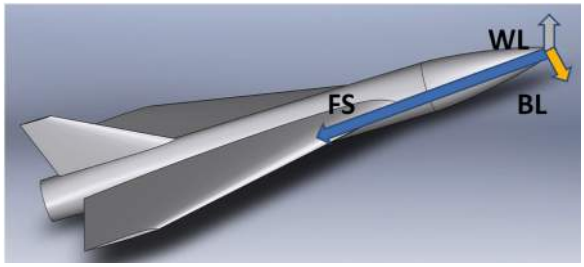

Figure 1 - Aircraft "Lofting" Coordinates (*FS,BL,WL*) and sign convention

We size primary structure using a rule-based method that considers the interplay between shear, tension, compression and buckling. For buckling, we consider the simple Euler-buckling problem of thin, unsupported wing skin panels as well as the overall Euler-buckling problem of a stiffened panel comprising the entire wing upper or lower "cover" structure (skin and stringers). Our method leverages many methods described in Niu [8][9]. We choose the skin thickness, the size of the wing spar caps, and the number and size of transverse wing stringers to develop a minimum weight wing. The structural design varies on a "bay-by-bay" basis; that is we hold the wing skin thickness, number and size of stringers constant between any two rib sets.

From this method, we can run complex trade studies documenting how disciplinary inputs from weight, performance, propulsion and materials groups can influence the weight and the physical design of a compliant wing. Although we search for the lowest weight, structurally feasible wing, our algorithm may fail to find any wing structure sufficient to withstand the loads. Our method has the ability to report the lack of feasibility and the location and cause of such design "troubles" to designer.

To verify the resulting preliminary structural design, we use application scripting capabilities to export our proposed geometry to both a solid model (rendered using *NX*) and to a finite element mode (*NX NASTRAN*). *NX* produces both solid and surface models of the geometry. The solid model is used for purposes of visualization and more importantly, weight calculations given the density properties of the material used during the rule-based sizing process. The surface model is idealized and exported to *NX NASTRAN* to be meshed and finally the material, loads and constraints can be applied to simulate the desired validation conditions. Displacement and stress results from this simulation are used to validate the theortical rule-based sizing method.

Once we sucesfully validated our structural design method over a broad series of test problems, we may use it to support either the detailed design and development of a specific configuration OR use it to develop basis data to understand trends and build "meta-models" of structural weight that can supersede the purely empirical weight equations found in sources like Torenbeek [5] or Raymer [1].

This paper will provide a detailed documentation of our rapid design procedure. It will include equations, algorithms and a discussion of all "empiricism"s incorporated into this rapid design process.

A. Basic Planform, Loading Cases, Material Properties and Design Variables

The wing design structure will be predicated upon an outer-mould-line "loft" and "design loading" cases.

We will size the wing structure to a series of flight loading cases. These include: 1) flight loads based upon a maximum flight weight, *MTOW*, and a design load factor in terms of positive (NZ_{max}) and negative (NZ_{min}) g forces and 2) ground loads based upon a maximum landing weight, *MLW*, and a negative (NZ_{min}) g force applied at the landing gear frame ribs. Flight envelope load factors are specified by the FAA in 14 CFR § 25.337 [10].

Material properties are given by the sorts of properties found in MIL HDBK-5J [11]. In other words, isotropic properties representing bulk characteristincs including the tensile yield strength (σ_{ty}), compressive yield strength (σ_{cy}), ultimate shear strength (σ_{su}), elastic modulus (E) and density (ρ). These properties may be derated as necessary by the statutory factor-of-safety (FOS) given by the FAA in 14 CFR § 25.303 [12] (typically 1.5). Thus the derated material characteristics are:

$$\sigma_{ty\_derated} = \sigma_{ty}/FOS \quad (1)$$
$$\sigma_{cy\_derated} = \sigma_{cy}/FOS \quad (2)$$
$$\sigma_{su\_derated} = \sigma_{su}/FOS \quad (3)$$

We define the wing planform as a modified symmetrical trapezoidal shape upon which reference values are computed. The basic planform is designed in terms of a wing-tip to wing-tip overall span (b), a basic trapezoidal taper ratio (*TR*) which is defined as the ratio of tip to root chord of the basic trapezoid, a mid chord sweep ($\Lambda_{c/2}$) angle of the basic trapezoid as well as arbitrary spanwise chord function ($c(y)$) which allows for "yehudis," raked wingtips and other non-trapezoidal planform modificaitons. Similarly, the overall wing thickness is defined in terms of an arbitrary spanwise wind referenced thickness to chord ratio ($t/c(y)$); see Figure 2.

Thus, the actual maximum thickness of the wing section may be defined in terms of the arbitrary functions $(t/c)(y)$ and $c(y)$ as:

$$t(y) = \left(\frac{t}{c}\right)(y) * c(y) \quad (4)$$

Whereas the spar locations are predicated on a spanwise invariant percentage chord location based upon the fundamental trapezoidal planform. Typically the front spar is located at the 15% chord point; the rear spar at the 65% chord point. Thus, the distance between the spars is:

$$dist_{betweenspars}(y) = 0.5\, c(y) \quad (5)$$

From this geometry (depicted in Figure 3), the reference area (*Sref*) and aspect ratio (*AR*) may be defined as follows, where:

$$Sref = b \cdot \bar{c} \quad (6)$$
$$AR = b/\bar{c} \quad (7)$$
$$TR = c_{tip}/c_{root} \quad (8)$$

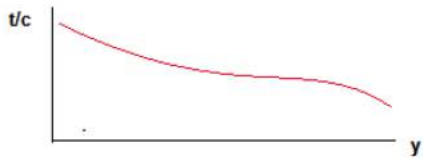

Figure 2 – Sketch of spanwise variation in wing thickness to chord ratio (t/c).

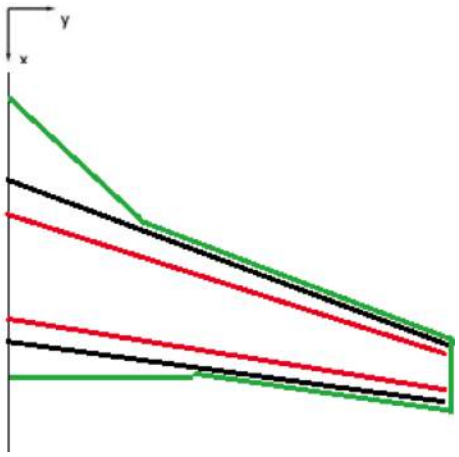

Figure 3 – Sketch of the trapezoidal basis for wing spar locations superimposed upon an arbitrary cranked planform. The arbitrary planform is shown in green, the fundamental trapezoidal geometry is shown in black, the spar locations are shown in red.

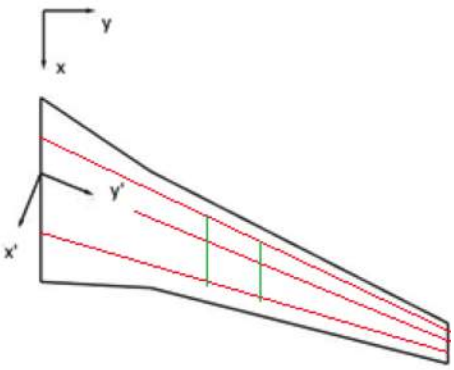

Figure 4 – Sketch of the mid-chord-sweep aligned structural coordinate system (x' – y') as opposed to the global lofting coordinate system (x – y). Spar and stiffeners are called out in **red**. Rib locations are called out in green.

and

$$\bar{c} = 1/2(c_{tip} + c_{root}) \qquad (9)$$

Refer again to Figure 3. This formulation allows us to represent the wing in terms of a local coordinate system oriented with the mid chord sweep. In this system, the structural semi-span of the wing (that aligned with the *y'* coordinate axis) is defined as:

$$(\frac{b}{2})_{structural} = (\frac{b}{2})/\cos(\Lambda_{c/2}) \qquad (10)$$

In addition to specifying the location of the front and rear spars, we may define the rib-to-rib spacing of the wing primary structure in terms of a spanwise distance, *Δy*; these too may be seen in Figure 4 (above). Thus, the presence of wing sweep alters the length of unsupported panels in the structural, *y'*, axis:

$$\Delta y' = \Delta y/\cos(\Lambda_{c/2}) \qquad (11)$$

A real wing will have finite weight, which will provide inertial relief against lift induced shear and bending moment. To determine design loadings the weight of the wing must be taken into account.

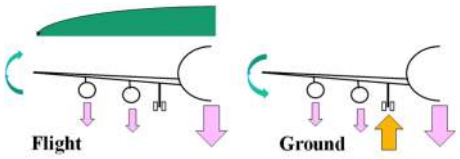

Figure 5 – Sketch of the shear and bending moment arising from wing structural and non-structural mass under flight and hard-landing loading conditions.

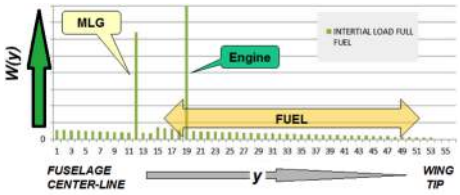

Figure 6 – Sketch of a "lumped mass" model comprising wing sturcutral and non-structural mass under a nominal 1-g loading.

The weight distribution consists of

(1) basic wing structure
(2) power plants
(3) landing gear, if mounted on the wing,
(4) other heavy items (i.e. fuel, flap actuators, flaps, ailerons)

Because at "in flight" conditions (positive *Nz* operation), fuel and engine weight is a relieving load, a considerable structural savings may result from the reduction in loading. However, in a hard landing these lumped and distributed weights work against the designer (see Figure 5).

We will use a "lumped mass" approach to defining the weight of the wing. The wing weight will be defined as a function of semi-span location. It will comprise continuous loads (a "smeared" representation of the weight of flaps, leading edges, fuel and a primary structure) plus discrete point loads (representing engines, pylons, the landing gear, etc.). Together they will define a weight distribution, *W(y)*; see Figure 6.

B. Integrating Basic Loads into Shear and Bending Moment and Bending Torque

To render this method computationally tractable, we specify an analytical transverse aerodynamic load distribution. For purposes of these trades, we presume wings develop an "elliptical" transverse load at both the *Nzmax* (positive load factor limit) and *Nzmin* (negative load factor limit) case. If desired in the future, itt is relatively straightforwards to replace this formulation with higher fidelity span loading distribution.

In general, the aerodynamic load distribution is defined as:

$$L'(y) = C_L(y) q\, c(y) \qquad (12)$$

Where $C_L(y)$ represents the section lift coefficient, C_L, as a function of the butt-line,y.

Thus, the integrated load of the wing can be found integrating this function from wing-tip to wing-tip:

$$L = \int_{-b/2}^{+b/2} L'(y)dy \qquad (13)$$

Recall that from a structural design standpoint, the global lofting coordinates (*x,y,z*) are less applicable. It is better, if we are to consider the wing as some form of equivalent beam, aligned with axis of structural sweep, to compute shear and bending moment in terms of the transformed coordinate system, *x',y',z'*. Thus, the relevant shear and bending moment functions arising purely from aerodynamic loads are of the form:

$$\tau'(y') = \int_{y'}^{(\frac{b}{2})/\cos(\Lambda_c)} Nz\left(L'(\breve{y}') - W'(\breve{y}')\right)d\breve{y}' \qquad (14)$$

and

$$M'(y') = \int_{y'}^{(\frac{b}{2})/\cos(\Lambda_c)} \tau'(\breve{y}')d\breve{y}' \qquad (15)$$

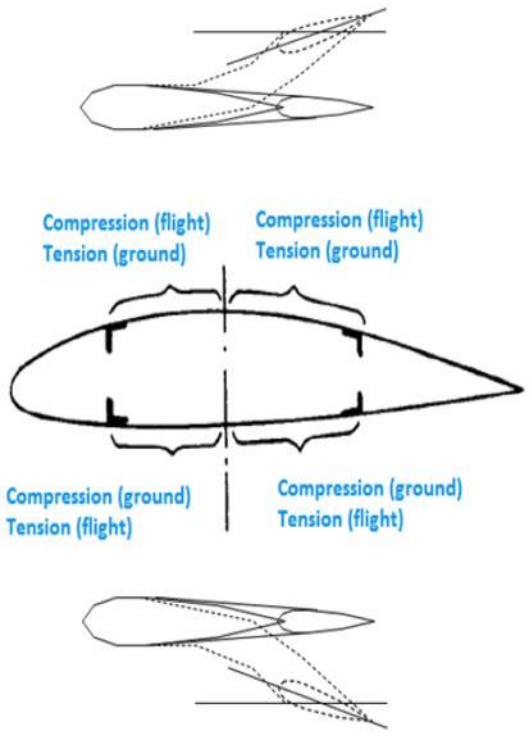

Figure 7 – Sketch describing "envelope" loading situations (+Nz flight vs. –Nz ground)

Where for purposes of simplification, *L'(y')* is the 1-g flight load distribution at the design loading condition, *W'(y')* is the 1-g weight distribution at the design loading condition, and *Nz* is the design load factor. The three most important "envelope" load cases comprise: 1) a maneuver at positive, *Nzmax*, (typically *Nzmax=2.5-g's*) at maximum take-off-weight, *MTOW*, with the maximum payload and the least favorable (minimum and inboard weighted) fuel loading in the wing, 2) a maneuver at negative, *Nzmin*, (typically *Nzmin=-1-g*) at maximum take-off-weight, *MTOW*, with a minimum payload and a full fuel load in the wing, and 3) a hard-landing at *Nz=-3-g's*, at maximum landing weight, *MLW*, with a minimum payload and the greatest possible fuel load in the wing. Each case stresses the wing structure to the sort of "worst case" loading event the aircraft is likely to encounter in operation.

Referring to Figure 7, positive flight design load factors are always higher than for negative flight design load factors. Thus, under the limiting case of positive gee's in flight, aero loads bend the wing tips "up." Thus, the wing upper surface is usually critical for compression loads while the wing lower surface sees peak tension loads. Alternatively, under a hard landing condition, the wing tips bend "down." The wing lower surface sees critical compression loads. The wing upper surface sees peak tension loads.

C. In-Plane vs. Overall Bending Torque; Converting into "Envelope Loads" in Upper and Lower Covers

The wing's torque box (comprising the upper and lower surface skins, spar caps and spar webs) must resist all imposed moments (both the transverse bending moment and torsional moments resulting directly from wing camber or indirectly from wing sweep). Wings experience aerodynamic forces normal to the local orientation of the wing, rather than forces directly opposing weight. Because a transversely loaded swept wing (without any torsional loading from wing camber) still develops an overall pitching moment about the wing-body-root, the indirect, wing sweep induced torsion cannot be neglected. Thus, a simplified root-bending-moment formulations (even one including the "structural span") does not fully capture the structural design challenge.

While we computed "in-plane" (*y'* reference axis) bending moments in equation 13, the net bending torque distribution comprising secondary bending torque components induced indirectly as a result of sweep is:

$$T'(y') = \int_{y'}^{(\frac{b}{2})/\cos(\Lambda_c)} \tau'(\breve{y}')\sqrt{(1+\sin(\Lambda_{c/2})^2)}d\breve{y}' \qquad (16)$$

Note that for an unswept wing ($\Lambda=0^o$), the net in-plane bending torques are identically equal to the transverse bending moment of the wing.

Neglecting buckling concerns, the wing torque box must locally and globally withstand all aerodynamically applied torques without yielding in tension or compression. This provides a means to determine the lower bound, the minimum cross sectional area of the upper or lower covers. If, for buckling reasons, additional material is needed, the stiffened panel will be heavier than needed to resist simple tension loading.

In our computational application, applied forces and moments were computed at discrete spanwise stations, i, representing the unsupported wing section between two adjacent chordwise ribs. Our nomenclature locates "Wing Station 1" along the fuselage centerline, and wing station n at the wing tip.

D. Computing Minimum Cross Sectional Area of the Upper and Lower Covers

Any given bending moment (or torque) can be resolved into an individual force couple, of equal and opposite forces, P, acting over a distance, d. (refer to Figure 8)

$$T = P\ d \tag{17}$$

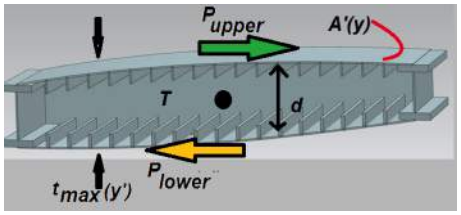

Figure 8 – Sketch resolving wing bending moment into forces along the upper and lower wing covers (comprising the spar caps, skin and any stiffeners)

For a typical wing, comprising a NACA 4-digit thickness form with the front spars located at 15% chord and the rear spar located at the 65% chord point; the "average" distance between upper and lower wing covers is only 70% of the magnitude of the maximum thickness of the wing. Thus, the tension and compression forces in respective lower and upper wing covers are equal to the torque divided by 0.70 of the local wing section thickness:

$$P = \frac{T}{d} \xrightarrow{yields} P(y') = +/- \frac{T(y')}{0.70\ t(y')} \tag{18}$$

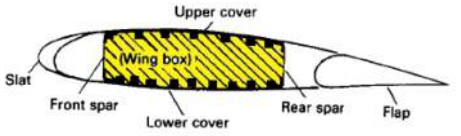

Figure 9 – Sketch resolving the torque box into spar caps, skin and any stiffeners

As shown in Figure 7, above, for positive Nz cases, the wing lower cover will be in tension and the wing upper cover will be in compression. The opposite holds true for negative Nz cases. The wing lower cover will be in compression; the wing upper cover will be in tension.

Thus, for a given material yield strength, σ_{ty}, the structure can withstand a tensile force proportional to the material area in upper and lower covers. Thus, the tensile strength limited cross-sectional area, A, of the upper or lower covers (sliced in a chord-wise plane) is:

$$A_{upper\_and\_lower\_cover} \geq P(y')/\sigma_{ty} \tag{19}$$

Substituting equation 18 into 19 results in the following relationship:

$$A_{upper\_and\_lower\_cover} \geq T(y')/(0.70\ t(y')\ \sigma_{ty}) \tag{20}$$

The relevant torque box area, $A_{upper\_and\_lower\_cover}$, for this computation comprises the following "bending resistant material." Refer to Figure 9. The spar usually looks like a modified "I" beam where the vertical "stroke" of the "I" is the spar web (typically quite thin) and the top and bottom "strokes" of the "I" the spar caps. The spar & spar caps may be integrally machined or built up out of smaller pieces, welded or riveted together.

Thus, when the wing resists transverse bending the spar caps and skin carry the majority of the stresses (as opposed to the spar webs) because the spar caps are furthest from the shear center of the equivalent beam.

E. Computing the Sizes of the Upper and Lower Cover, Spar Webs and Rib Web Structure

Our computational strategy to develop a complete torque box geometry (that is to size the spar web, spar caps, skins and stiffeners) requires us to balance loads between spar caps, skins and main spar. Our algorithm will ensure that we do not violate five important constrants:

1. The ensemble will not exceed the tensile yield strength of the material on tension surfaces
2. The ensemble will not exceed the compressive buckling strength of the geometry on compression side stiffened panels
3. Individual "strips" bounded by chord-wise stiffeners and span-wise ribs will not buckle in compression
4. The spar web will sustain applicable wing shear forces without exceeding material shear strength limits
5. The rib webs will be scaled sustain applicable wing shear forces without exceeding material shear strength limits

This method makes certain assumptions (static determinacy is approximated by "crippling factors" to make up for some static indeterminacy in the built-up structure), but is computationally tractable.

Thus to size the wing structure on a "bay-by-bay" basis, we must size the following elements, based upon the aforementioned constraints.

1. The **upper cover** (skin and stiffeners) will be sized for tensile strength from ground loads and Compressive stability (buckling) from flight loads
2. The **lower cover** (skin and stiffeners) will be sized for tensile strength from flight loads and compressive stability (buckling) from ground loads
3. The **spar caps** will be sized based upon tensile strength from ground loads traded against the overall Compressive strength and structural stability required by flight loads (the spar cap sizing can be traded off against the number and size of stiffeners)
4. The **spar web** is sized for tensile and compressive strength resisting primary wing bending as well as fuel slosh / crash loads

To determine the optimum sizing, an algorithm will be written to "grow" the wing from root to tip. For each "bay" between two neighboring ribs, the alogirthim enumerates all possibile combinations of upper cover geometry, lower cover geometry and spar geometry. For each possible design, relevant critical loading conditions will be established and compared against estimated loads. From this collection of possibilities, the algorithm selects the minimum weight configuration that satisfies all feasibility criteria.

In our implementation, we specify a rib-to-rib spacing distance as well as a stringer-to-stringer spacing distance as independent design variables that remain constant over the entire wing.

We then allow the computer to enumerate 30 discrete possible spar cap sizes (from 1-inch wide by ¼-inch thick to 8-inches wide by 2-inches thick), 40 discrete possible skin thicknesses (from 18 gauge aluminum through 1-inch) and 20 discrete stringer geometries (from 1x skin-thickness wide by 2x skin-thickness tall to 2x skin-thickness wide by 8x skin-thickness tall). From this enumerated set of 24,000 possibilites (per "bay)" we then dismiss all geometries where by the overall cross-sectional-area of the implied geometry is less than Aupper_and_lower_covers as governed by equation 18, supra.

We make a bold assumption that the stiffened skin panels are statically determined, and thus, share a fraction of the total load proportional to their cross-sectional area. From this, we can infer from the compression load as applied to the entire stiffened panel, component compression loads as applied to individual spar caps, the skin, an individual stringer or to the unsupported stip of skin between two stiffeners.

Our stiffened panel buckling criteria follows Niu [8], thus:

$$P_{cr\_stiffened\_panel} = \pi^2 \, E \, \left(\frac{\rho^2}{L^2}\right) A_{stiffenedpanel} \tag{21}$$

where

$$A_{stiffenedpanel} = thickness_{skin}\, dist_{spartospar} + \#_{stringers}(height_{stringer}\, thickness_{stringer}) \quad (22)$$

$$L = dist_{ribtorib} \quad (23)$$

and the radius of gyration, ρ, is described by:

$$\rho^2 = (b^2 \left(\frac{d}{b}\right)^3 \left(\frac{Ts}{t}\right))/(12\ \left(1 + \left(\frac{d}{b}\right)\left(\frac{Ts}{t}\right)^2\right)\left(4 + \left(\frac{d}{b}\right)\left(\frac{Ts}{t}\right)\right)^2 \quad (24)$$

with the following relationships:

$$b = dist_{spartospar}/(\#_{stringers} + 1) \quad (25)$$
$$d = height_{stringer} \quad (26)$$
$$Ts = thickness_{stringer} \quad (27)$$
$$t = thickness_{skin} \quad (28)$$

If this critical value, *Pcr*, exceeds 150% of the actual compression force applied to the stiffened skin, the algorithm considers the net design infeasible, and moves on to examine another enumerated possibility.

Our Local Strip Buckling also follows a procedure recommended by Niu [8]. It employs the Euler Strip Buckling Equation using NASA factors for a strip where all edges are effectively clamped and fully supported.

$$P_{cr\_strip} = 6.3\ E\ \left(\frac{t^3 W}{b^2}\right) \quad (29)$$

where

$$W = dist_{spartospar}/(\#_{stringers} + 1) \quad (30)$$
$$t = thickness_{skin} \quad (31)$$
$$b = dist_{ribtorib} \quad (32)$$

If this critical value, *Pcr*, exceeds 150% of the actual compression force applied to the stiffened skin, the algorithm considers the net design infeasible, and moves on to examine another enumerated possibility.

We can thus find a design that simultaneously satisfies compression yield, tension yield, stiffened panel buckling and local strip buckling constraints.

In order to size spar webs and rib webs for the shear loading condition, recall that the peak shear stress in a thin plate is effectively:

$$\sigma_{s\_max} = 1.5\ (\frac{\tau}{b\ h}) \quad (33)$$

where, τ is the applied shear, *b* is the web thickness and *h* is the physical height of the plate.

Spar webs must support shear generated by the aero loads of the wing. Because a multi-spar wing is a statically indeterminate structure, the load sharing between spars isn't clearly defined. Our "best practice" assumes that each spar could be responsible for the entire shear load.

Thus, the spar web thickness for any given bay is proportional to the peak shear force that the wing must resist and inversely proportional to the "height" of the aft spar web. On an typical NACA 4-digit section, the maximum thickness point on the form is found around the 30% chord point; the front spar height is 80% of the maximum section thickness. The more critical rear spar height is typically only 60% of the magnitude of the maximum thickness of the wing.

Thus the rear spar height controls the spar web thickness:

$$thickness_{sparweb}(y') = 1.5\frac{\tau(y')}{(0.6\,t(y'))\sigma_{su}} \tag{34}$$

where $t(y') = (t/c)(y')\,c(y)$ and σsu is the derated maximum allowable shear strength of the material.

Rib webs must tie the upper and lower covers together. Their shear forces are driven by the net loads acoss wings top and bottom.

$$thickness_{rib_{web}}(y') = 1.5\frac{\tau(y')}{\left(0.6\,dist_{betweenspars}(y')\right)\sigma_{su}} \tag{35}$$

Following this procedure, our algorithm develops the minimum weight torque box geometry (sizing the spar web, spar caps, skins and stiffeners, requires us to balance loads between spar caps, skins and main spar) of a "feasible" wing. Our final, coded optimization algorithm also includes some heuristics to keep the size of structural elements from "oscillating" from one bay to the next.

In the next section we will document our validation effort.

III. Initial Validation and Verification

For our initial validation cases, we will design a wing to an approximate wing geometry and flight performance characteristics to represent an early production B737 [13][14].

Test Case # 1 comprises:

1. Maximum Take-Off Weight (116,000-lbm) used to calculate the $+Nz_{max}$ envelope load case (wingtips bend upwards)
2. Maximum Landing Weight (92,800-lbm) used to calculate the $-Nz_{min}$ envelope load case (based on a 3-g hard landing) (wingtips bend downwards)
3. Design Nz_{max}=+2.5 g's
4. Design Nz_{min}=-1.0 g (flight), -2.5 g's (ground)
5. Wing Span, b=93-ft (tip-to-tip)
6. $Sref$ = 980-ft^2
7. Taper Ratio, TR = 0.279
8. Aspect Ratio, AR = 8.825
9. Wing Chord (See Figure 10a)
    a. Centerline Chord, C_0 = 16.5-ft
    b. Tip Chord, C_t = 4.6-ft
10. Thickness to Chord Ratio, $t/c(y)$ = 10% uniform (we note this as a simplification over the actual geometry) (see Figure 11a)

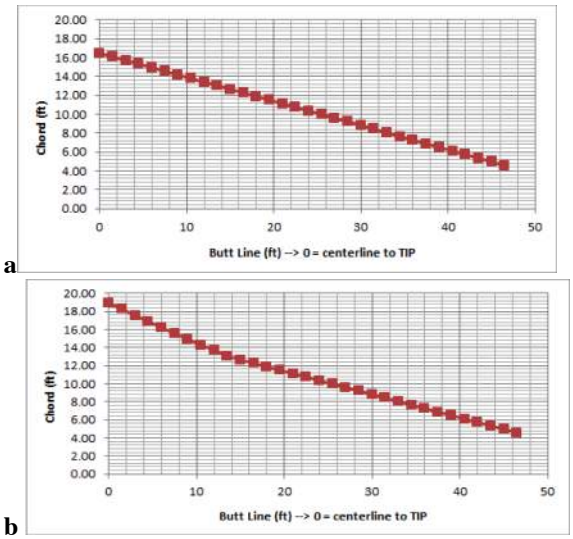

Figure 10 – Wing Chord Distribution. a) Test Case #1 (737 sized wing with simple trapezoidal planform) and b) Test Case # 2 (more realistic B737 wing)

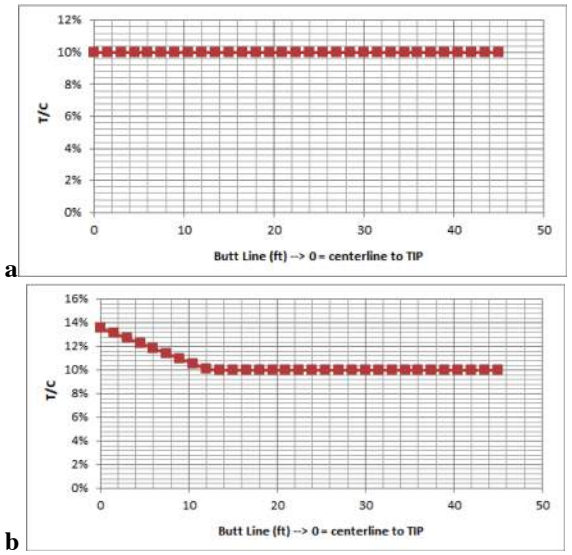

Figure 11 Aerodynamic Thickness to Chord Ratio – Spanwise Distribution – $(t/c(y))$ – nominal narrow-body-transport configuration

11. Distance between spars = 50% of trapezoidal planform
    a. Front Spar @ 15% chord of trapezoidal planform
    b. Rear Spar @ 65% chord of trapezoidal planform
12. Rib to Rib Spacing, 18-in BL in overall aircraft coordinate frame
13. Nominal Stiffener Spacing, 4-in FS in overall aircraft coordinate frame

Thus, this simplified test case lacks any credit for inertial relief due to structural (torque box) or non-structural mass (engines, fuel, landing gear) on the wing.

Test Case # 2 comprises:

1. Maximum Take-Off Weight (116,000-lbm) used to calculate the $+Nz_{max}$ envelope load case (wingtips bend upwards)
2. Maximum Landing Weight (92,800-lbm) used to calculate the $-Nz_{min}$ envelope load case (based on a 3-g hard landing) (wingtips bend downwards)
3. Design Nz_{max}=+2.5 g's
4. Design Nz_{min}=-1.0 g (flight), -3.0 g's (ground)
5. Wing Span, b=93-ft (tip-to-tip)
6. $Sref$ = 980-ft^2
7. Taper Ratio, TR = 0.279
8. Aspect Ratio, AR = 8.825
9. Wing Chord (See Figure 10b)
    a. Actual Centerline Chord, 19-ft
    b. Trapezoidal Planform Centerline Chord, C_0 = 16.5-ft
    c. Trapezoidal Planform Tip Chord, C_t = 4.6-ft
10. Thickness to Chord Ratio, $t/c(y)$ = 14% at root, tapering to 10% at 30% semi-span and holding this value to the tip. (see Figure 11b)
11. Distance between spars = 50% of trapezoidal planform
    a. Front Spar @ 15% chord of trapezoidal planform
    b. Rear Spar @ 65% chord of trapezoidal planform
12. Rib to Rib Spacing, 18-in BL in overall aircraft coordinate frame
13. Wing Bending Moment Relief
    a. Overall Structure: 12% of overall aircraft maximum take-off weight
    b. Fuel Load: 49,000-lbm overall (24,500-lbm per semi-span) distributed between 10% and 80% semi-span
    c. Engine & Pylon: 4300-lbm at 26% semispan
    d. Landing Gear @ 15% semispan

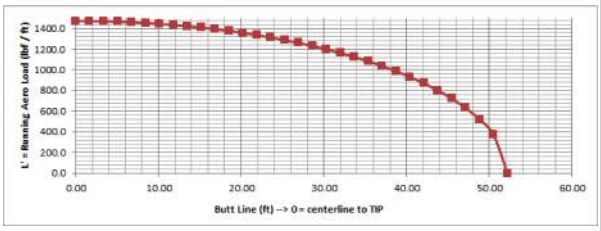

Figure 12 – Aerodynamic (elliptical) load distribution comprising 116,000-lbf net lift (58,000-lbf lift per semi-span) used in Test Case #1 and 2

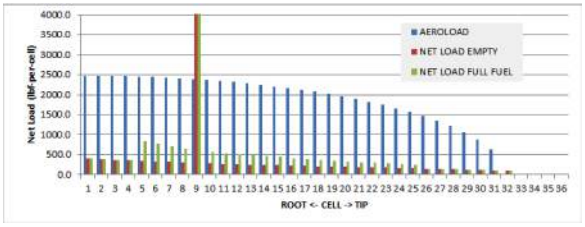

Figure 13 – Lumped Aerodynamic (elliptical) load and opposing inertial loads used in Test Case #2.

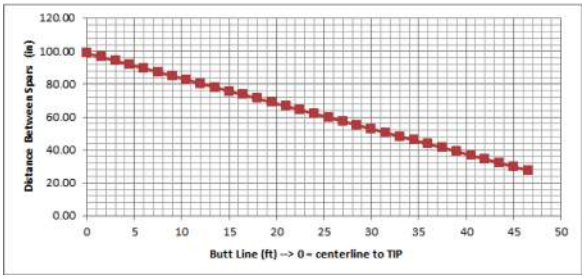

Figure 14 – Distance Between Spars – B737 type geometry - Test Case #1 and 2

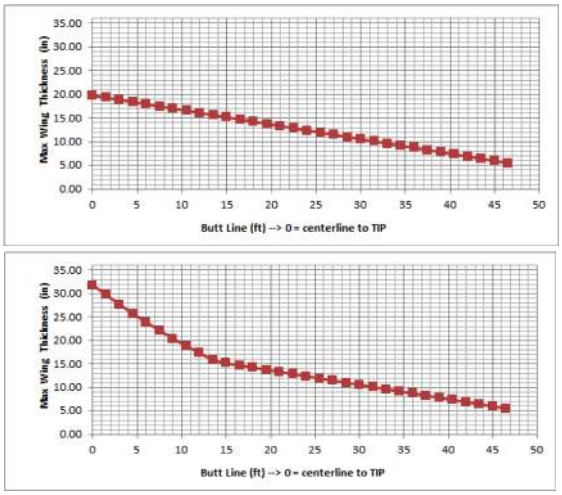

Figure 15 – Maximum Wing Thickness. a) Test Case #1 (737 sized wing with simple trapezoidal planform) and b) Test Case # 2 (more realistic B737 wing)

Thus, this test case has a more representative geometry for a wing with a "Yehudi" and includes credit for inertial relief due to structural (torque box) or non-structural mass (engines and fuel) on the wing.

A. Basic Aerodynamic Loads

Our design load case will be that of an elliptical transverse span load that integrates to represent flight at the design maximum takeoff weight. The distribution is common to both test wings, and is shown in Figure 12, above.

B. Inertial Loads

The counterpoint between aerodynamic and inertial loads for Test Case #2 is revealed in Figure 13. For this illustrative example, we assume that the overall wing (including structural, as well as the non-structural mass of flaps, leading edges, ailerons, actuators, antennae, fairings, fuel system but less the weight of engine and pylon) weighs 12% of MTOW. i.e. *Wwing* = 13,920-lbm for an aircraft with MTOW = 116,000-lbm. For this example problem, we distribute this weight as a uniform grid of lumped masses spaced evenly across the span.

In addition, we add specific interial lumped masses of to represent each engine. We expect each engine & pylon assembly to weigh 4300-lbm. For the purposes of Test Case #2, it is hung at 26% semi-span; BL=12-ft.

We also assume that the fuel is distributed proportional to the volume of each wing "bay" – that is the volume displaced between front and rear spar web, upper and lower wing cover and inboard and outboard rib. For Test Case #2, fuel can be contained between BL=3 and 36-ft.

The landing gear is placed at 15% semi-span (i.e. BL=7.5-ft). For this initial model, the landing gear does not provide appreciable inertial relief for flight at +*Nzmax*.

C. Material Properties

For these examples worked in this paper, we will utilize aluminum [11] with the following characteristics:

- Youngs Modulus, E = 10,700,000 lbf/in^2
- Density, π = 0.1 lbm/in^3
- Tensile Yield Strength, σ_{ty} = 44,000-lbf/in^2
- Compressive Yield Strength, σ_{cy} = 44,000-lbf/in^2
- Ultimate Shear Strength, σ_{su} = 38,000-lbf/in^2

Thus, applying the customary 1.5 factor-of-safety [12], under design loading conditions the aircraft structure should not exceed:

- Tensile Yield Strength, σ_{ty_derate}=29,300-lbf/in^2
- Compressive Yield Strength, σ_{cy_derate}=29,300-lbf/in^2
- Ultimate Shear Strength, σ_{su_derate}=25,300-lbf/in^2

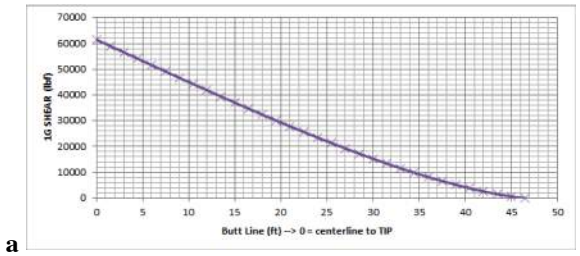

Figure 16 – Shear force at *Nz*=+1 as a function of global BL location. a) Test Case #1 (simple trapezoidal planform) and b) Test Case #2 (B737-like wing) for *Nz*=+1 and -1 cases.

Therefore, when looking a von Mises stress contour outputs from the finite element solution, we expect von Mises stress levels under the analyzed loading condition not to exceed ~29,000-lbf/in^2.

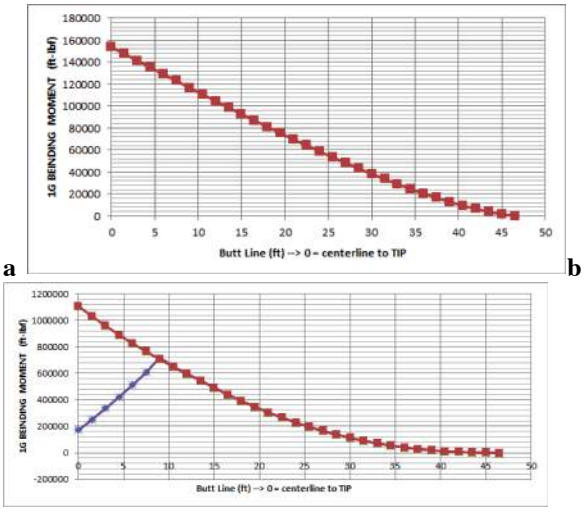

Figure 17 – Transverse Wing-Plane Bending Moment Magnitude *M'(y)* as a function of global BL location. a) Test Case #1 (737 sized wing with simple trapezoidal planform) and b) Test Case # 2 (more realistic B737 wing) for *Nz*=+1 and -1 cases.

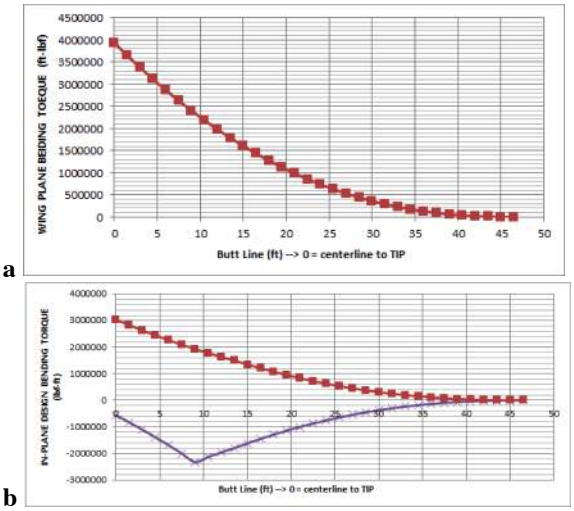

Figure 18 – Integrated overall "in-plane" bending "torque" *T'* at design +Nzmax as a function of BL location. a) Test Case #1 (737 sized wing with simple trapezoidal planform) at *Nz*=+2.5 gand b) Test Case # 2 (more realistic B737 wing) for *Nz*=+2.5 and -3.0 g

D. Key Derived Geometry

The geometry of the wing primary structure (its torque box) derives from the outer-mould-line geometry. The distance between spars can be inferred from the trapezoidal, planform geometry and the percentage chord locations of the forward and aft spar. As shown in Figure 14, this distance is common between test case #1 and #2 geometries.

The depth of the torque box across the span is related to the shape of the thickness form scaled by the maximum thickness of any given streamwise section (see Figure 15, supra). Because of the trailing edge chord extension behind the rear spar alters the physical planform (Figure 10b) and the spanwise variation in thickness-to-chord ratio (Figure 11b), Test Case #2's wing is physically thicker than Test Case #1 (compare Figure 15a to 15b).

E. Shear and Bending Moments

Following the Equations 14, 15 and 16, the net loads for test cases #1 and #2 integrate up into shear (Figure 16), bending moment (Figure 17) and net bending torque (Figure 18) as a function of butt-line location (*BL*). Note the difference between bending moment and bending moment for these cases. Recall, due to the 25° wing sweep of the Boeing 737, the transverse aerodynamic loads cross-couple between "in-plane" bending moments aligned with the principal bending axis of the wing (parallel to the *y'* axis) and torsional moments (about the *y'* axis) resulting from the swept wing being clamped at the root. In other words, a point load applied at the wing tip with both bend and twist a swept wing. A comparision between Figures 18a and 18b reveals the large reduction in shear experienced by the inboard wing due to the presence of inertial relief from structural and non-structural mass. Consequently, root bending torques (Figures 19a vs 19b) diminish by approximately 30%.

F. Optimizer Selected Design Parameters

The optimizing algorithm develops from Equation 18, a set of "envelope" or "worst case" tension and compression loads for upper and lower covers arise from the need to resist the bending moment across the couple equal in height to the physical thickness of the wing. The product of the tension (or compression) force and the usable tensile (or compression) yield force of the material represents the minimum cross-sectional area of the wing upper or lower cover (the skin + spar caps + stiffeners).

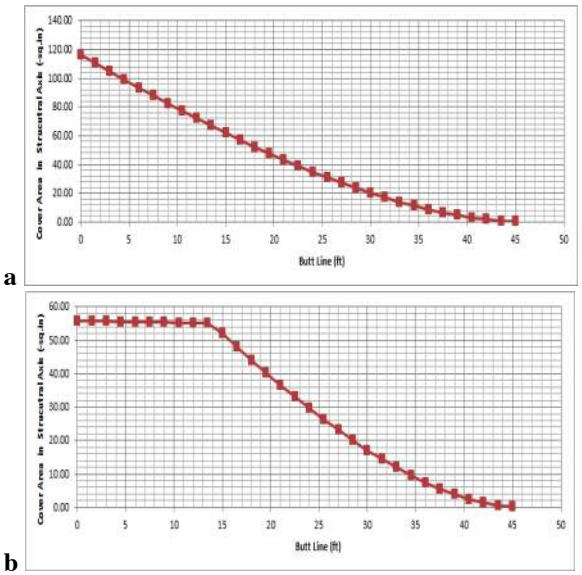

Figure 19 – Minimum Cover Area for Tension Loading Criteria to Resist Critical Envelope Loads. a) Test Case #1 (simple trapezoidal planform) for Nz=+2.5/-2.5g cases and b) Test Case # 2 (B737-like wing) for Nz=+2.5/-3.0g cases.

Under an ideal situation, this area may be divided between skin, spar caps and stiffeners, to produce a structure that can resist tensile and compressive material yield and avoid compression buckling problems at either local skin (or stiffened panel) levels (equation 20).

Figure 19 demonstrates that the physically "thicker" wing in Test Case #2 along with its intertial relief reduces the bending moments that the structure must resist. Thus Test Case #2 has a noticeably smaller required cover area for tension loading resistance. At the root, the cover areas are diminished by nearly 50% as opposed to the simpler wing geometry. This implies the potential for a large reduction in the structural mass of the torque box stemming from inertial relief.

Our iterative design process may find that a feasible solution requires an actual cover area (comprising a discrete topology of skin thickness, spar-cap sizing, stiffener sizing and configuration) greater than the minimum. This is determined on a bay-by-bay basis across the wing semi-span. Comparisons of optimizer selected designs with the minimum cover area are found in Figures 20a and 20b. While the simple, trapezoidal planform wing of Test Case #1 leads to a design where the actual cover area closely follows that sized by

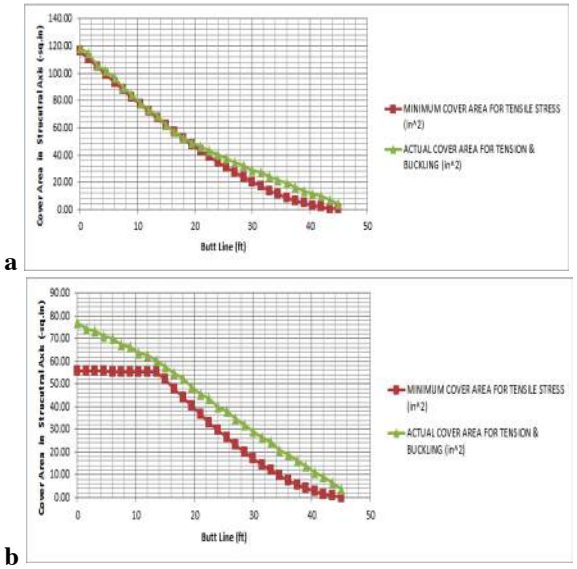

Figure 20 – Minimum Cover Area for Tension Loading Criteria vs Actual Cover Area needed to satisfy Tension, Compression, Stiffenened Panel Buckling and Local Panel Buckling Criteria while resisting Critical Envelope Loads. a) Test Case #1 (737 sized wing with simple trapezoidal planform) and b) Test Case # 2 (more realistic B737 wing)

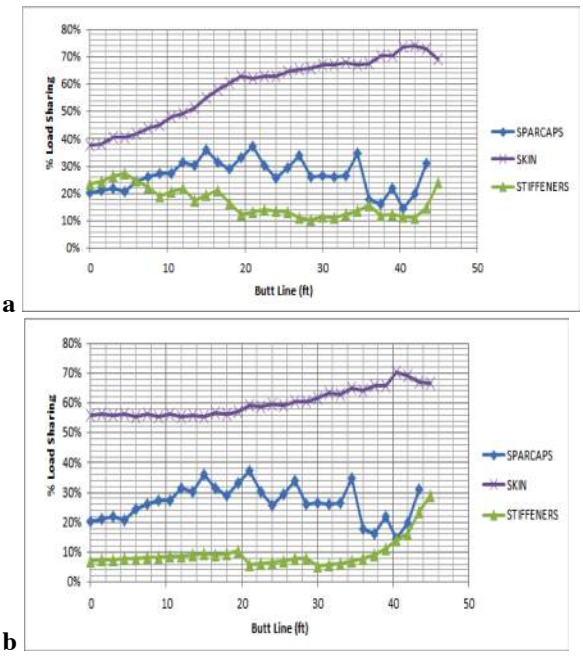

Figure 21 – % load sharing between skin, stiffeners and spar caps in "optimized" wing. a) Test Case #1 and b) Test Case # 2 (more realistic B737 wing)

tension in the upper surface covers, Test Case #2 substantiates a significantly lighter wing (but one where actual cover areas are substantially larger than that implied by simple, tension based strength sizing).

Assuming a statically determinate structure, the optimizer selected design will share load proportional to its cross-sectional area. The optimal structure is a semi-monocoque design, sharing loads between spar caps, skins and stiffeners. Figures 21 through 26 document the load sharing as well as the resulting dimensions of spar caps, skins and stiffeners as well as the number of stiffeners per wing "bay."

Compare Figure 21a with Figure 21b (see previous page). We see that once the optimizer has run its course, the recommended wing design for the simple geometry (Test Case #1) shares loads relatively uniformly between spar caps, skins and stiffeners. Test Case #2 results in a structure that carries much more load in the skins.

Conversely a comparison of Figure 22a with Figure 22b demonstrates that with reduced bending moments, the wing becomes dominated by local buckling concerns. Thus the optimizer counters this problem by off-loading the spar caps, and thickening the skins to compensate.

Inspection of Figure 23a as opposed to Figure 23b documents the choice of the optimizer in halving of the width of the spar caps (from 8-inches wide at the wing root to 4-inches wide) along with a radical thinning of the spar cap flange depth (from 2-inches thick at the wing root to 0.6-inches thick.

Inertial relief leads to the wing designed for Test Case #2 to actually have similar skin thicknesses to that designed for Test Case #1. Referring to Figure 24a as opposed to Figure 24b, the wing thickness does not change radically (both wings require approximately 1/2 –in thick skins at the root) but the spanwise "thinning" of the skins differs slightly between the two designs made for differing load cases.

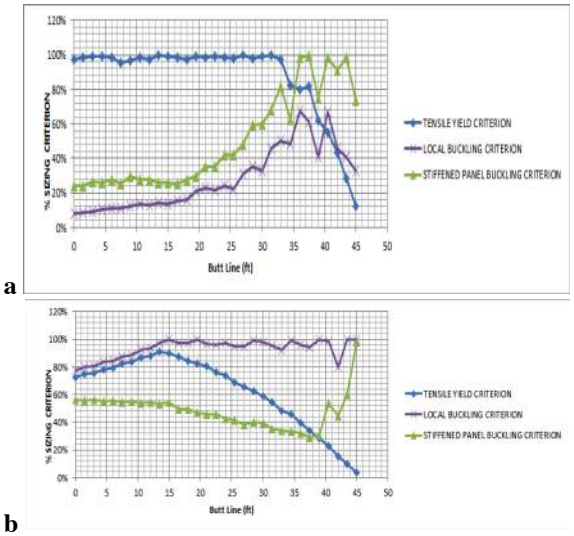

Figure 22 –sizing criteria for load sharing between spar caps, skin and stringers on optimized wing. a) Test Case #1 (simple trapezoidal planform) and b) Test Case # 2 (more realistic B737 wing)

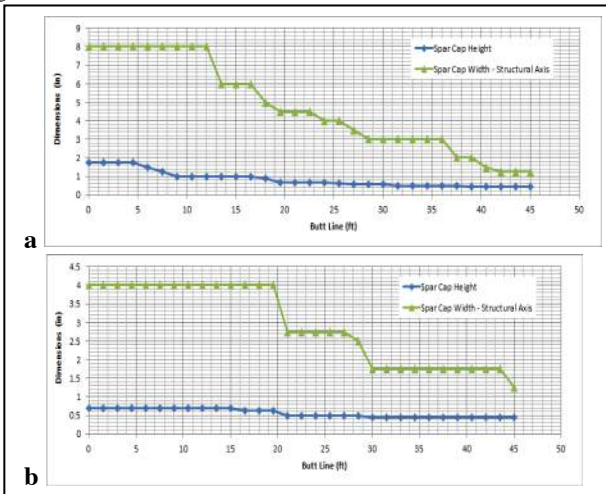

Figure 23 – Spar Cap Height & Width for algorithm selected optimized wing. a) Test Case #1 (737 sized wing with simple trapezoidal planform) and b) Test Case # 2 (more realistic B737 wing)

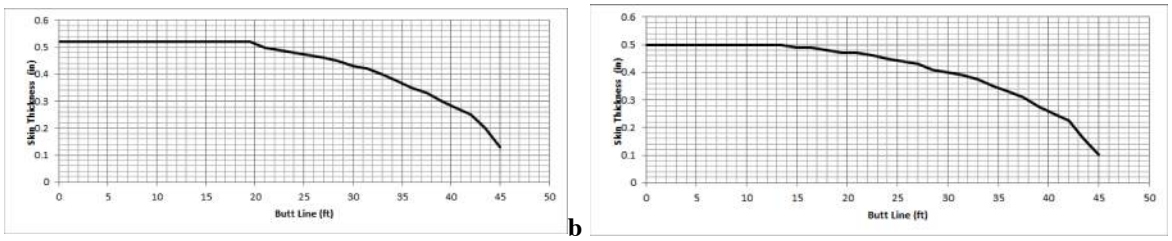

Figure 24 – Wing skin thickness for optimized wing. a) simplified geometry, b) B737-like geometry

Because the two test case wings share identical spar locations, rib spacing (18-in) and stiffener density (4-in chord wise spacing), the number of stiffeners does not differ between the two designs. Referring to Figure 25, both wings have 17 stiffeners per bay at the root and 5 stiffeners per bay at the tip. However, the optimizer selected sizing for the stiffeners varies considerably from wing #1 to wing #2 (see Figure 26a as opposed to 26b)

The wing designed for Test Case #1 weighs 10,488-lbm incorporating all criteria (tensile and buckling); if it were sized purely to tensile yield conditions it would weigh 9,862-lbm. The difference is a 6% penalty for adding the realism of buckling into this design.

The wing designed for Test Case #2 weighs 10,195-lbm incorporating all criteria (tensile and buckling); if it were sized purely to tensile yield conditions it would weigh 8,850-lbm. The difference arising from the inclusion of buckling constraints into the design amounts to a necessary 15% weight penalty. For example, if an aircraft were sized using a simplified tensile model, the actual production wing would likely experience at least a 1,350-lbm weight shortfall.

G. Validating the Design: Step # 1 - Building the NX Model

A wing geometry template in the form of a parametric 2D sketch begins the wing model creation process (see Figure 27). Inputs of reference area, tip-to-tip span, taper ratio, and sweep produce the trapezoidal outline of the wing. The parametric sketch will also produce outlines of the spars given % chord from the leading edge values of forward and aft spar, as well as a reference line positioned halfway between both spars where loads will later be applied. Dimensions of a kink (for a "Yehudi") and its location as a function of % span are included as parametric inputs. These inputs are directly entered into *NX* as *NX Expression* variables that have been defined within the model and control dimensions/constraints of the template sketch. Based on the rib-spacing set by the sizing spreadsheet, rib lines are populated. Lastly, spar cap outlines are constructed given widths and span placements produced by the spreadsheet.

With all the 2D outlines defined, 3D wing construction begins (see Figure 28). Given unitless airfoil coordinates, rib spacing, and maximum t/c % values per rib, we used a *VBA/Excel* spreadsheet to generate global airfoil coordinates of each rib section. This spreadsheet is embedded into the *NX* part file. An embedded spreadsheet can "call upon" the aforementioned *NX Expression* variables in order to produce the airfoil coordinates without having to re-

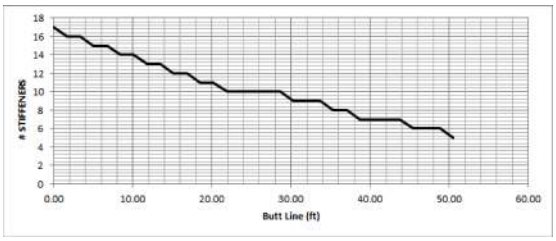

Figure 25 – - # Stiffeners for upper and lower covers for optimized wing.

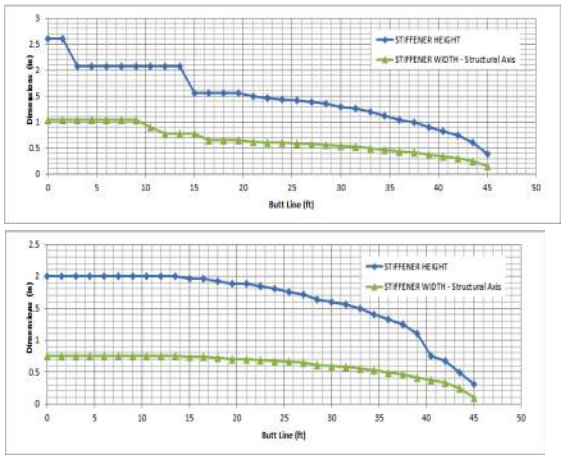

Figure 26 – - Stiffener sizing per bay (upper and lower) for optimized wing. a) simplified geometry, b) B737-like geometry

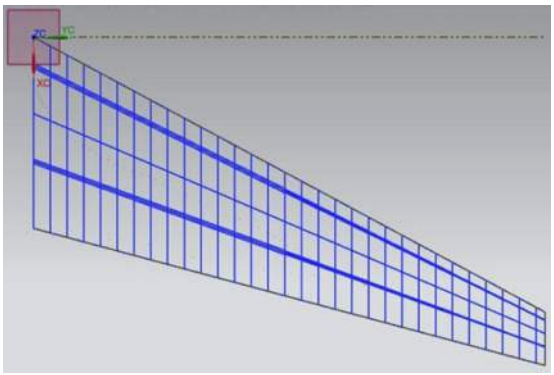

Figure 27 – Parametric 2D sketch used to generate outline of wing, with spar, spar cap, and rib outlines shown (Test Case #1 - Simplified Geometry)

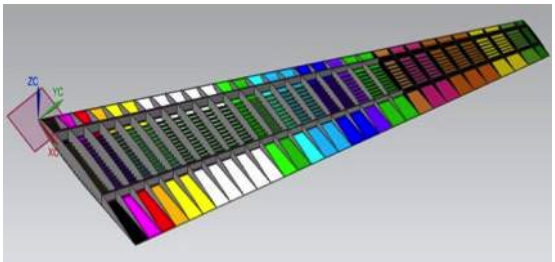

Figure 28 – Color-coded surface model of Simplified Geometry mock 737 wing with upper wing skin and stiffeners hidden so internal structure can be seen

enter them. A separate *VBA* script is then executed within *NX* that imports the global airfoil coordinates and creates an airfoil spline and a rib surface body bounded by the spline at every rib station. The script then lofts a wing skin surface over the ribs. Spars, spar cap, and stiffener surfaces are then created manually using extrusion and surface trimming commands with the 2D outlines. At the conclusion of the wing model build-up, all geometry is in the form of sheet bodies for meshing reasons that will be explained later.

H. Validating the Design: Step # 2 – Meshing the FEM grid

In preparation for finite-element meshing, each surface body is grouped and color-coded according to its thickness for convenient identification during the meshing process. Also, points are created at every intersection of the mid-spar line with a rib line and projected onto the lower wing surface. The flight loads calculated by the spreadsheet will applied at these points. This surface model is to be used for structural analysis. A second model is created where all surfaces are thickened into solids and a weight analysis can be performed given the material density.

An idealized version of the surface model is exported to *NX NASTRAN* for pre-processing. All edge-surface interactions are stitched together so that all the surfaces will share mesh nodes at these intersections. This allows for the proper transfer of stresses and displacements between all meshed surfaces. A 3D mesh generally needs several elements of "depth" from one surface to the next to produce reliable results. Given some of the small thickness values produced by the spreadsheet, achieving two to three 3D elements across a thickness less than a tenth of an inch would lead to an unnecessarily fine mesh and consequently high simulation time. For these reasons, it was decided to use 2D shell elements for meshing and this is why the model was constructed using sheet bodies. The selection of 2D elements meant that the spar caps had to be modeled as surfaces completely parallel to the spars and extending from the wing skin to the spar cap height specified by the spreadsheet.

Triangular 2D mesh elements were then chosen as the most appropriate element shape. Attempting to mesh the wing with quadrilateral elements led to an unacceptable number of elements that violated Jacobian or Warp threshold, especially when meshing the ribs and wing skins. Using triangular elements instead produced not a single "bad" element. However, traditional three-node triangular (*CTRIA3*) elements are constant strain elements and thus can result in overly stiff results. For this reason, *CTRIAR* elements were selected. CTRIAR elements include rotational stiffness in the normal out-of-plane direction making them linear strain elements [15].

Lastly, shell thickness values were set. For a larger wing model, the spreadsheet can produce upwards of sixty different thickness values meaning just as many mesh collectors are necessary. Furthermore, these thicknesses values are distributed over thousands of different sheet bodies. Since *NX* allows for the selection of objects based on color, the sheet bodies were color-coded when creating the model for convenient mesh thickness allocation. Specific mesh points are created at the skin and rib intersections points on the lower surface. These mesh points will be the locations of the applied loads. Lastly, material properties are assigned to the mesh collectors. The finite element model is then ready for application of loads and constraints for simulation.

The loads computed by the rule-based spreadsheet are applied to the meshed model at the aforementioned mesh points located on the lower wing surface with a positive global *z* direction. There is a load applied at every rib-skin intersection except for the most inboard rib; see Figure 29. The faces of the inboard rib are constrained so that all six degrees of freedom are fixed.

If we were to apply *Nzmin* loads, they would be placed at the same locations as are the *Nzmax* loads.

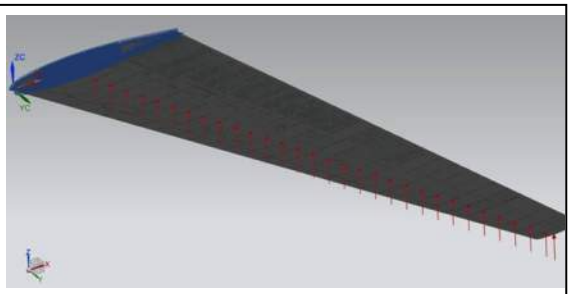

Figure 29 – *Nzmax* Loads and constraints applied to meshed mock 737 wing in *NX NASTRAN*

I. Validating the Design: Step # 3 –FEM solutions for Design Loading Cases

Here, we present simulation results for the *Nzmax* loading scenario for test case # 1. In Figures 301 through 32, this page and overleaf, we show elemental von Mises stress surface contours, the maximum of the contour plot was set to the maximum allowable stress dictated by the spreadsheet. The stresses plotted in the surface contours are the average/middle values between the two surfaces of the 2D shell elements. Internal stresses on the ribs, stiffeners, spars, and spar caps are also examined, as can be seen with internal stress results provided for the mock 737 wing. Displacement contour surface plots are also provided in Figure 31. As expected, maximum displacement occurs at the wing tips. Moreover, as this was a stress dominated sizing problem, we see a solution where the peak von Mises stresses locally approach the design limiting value of approximately 29,000 lbf/in^2 but never exceed this critical value.

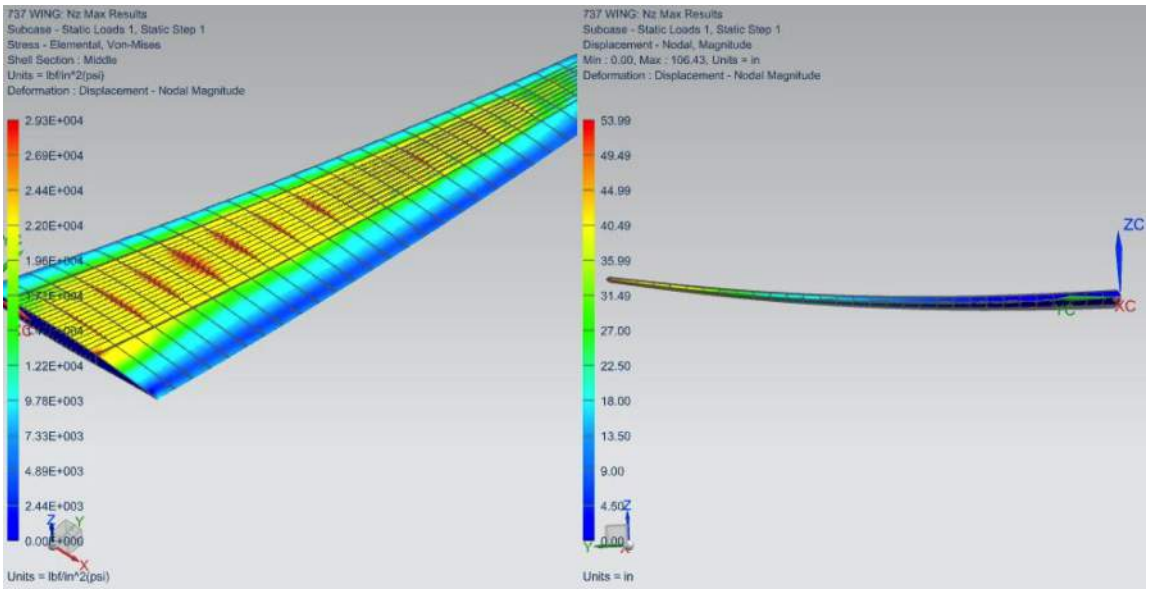

Figure 30 – von Mises elemental stress and displacement surface contours for Test Case # 1wing

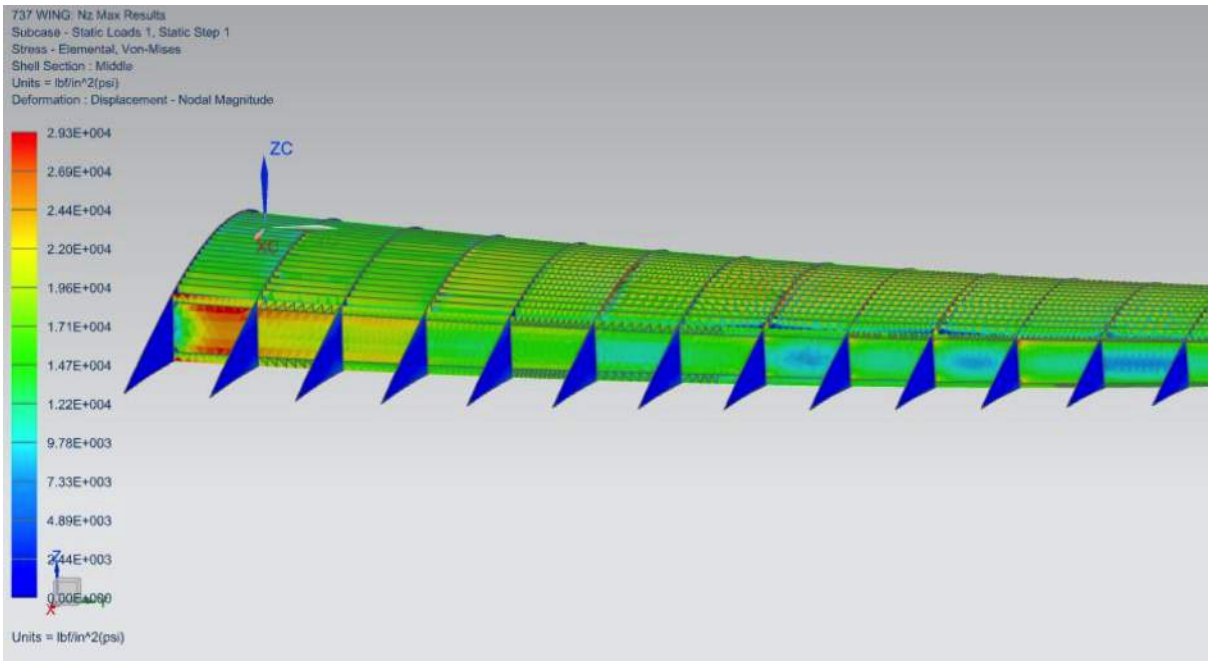

Figure 31– von Mises elemental stress surface contour on Test Case # 1wing, with wing skins hidden so that internal stresses on the aft spar web can be seen.

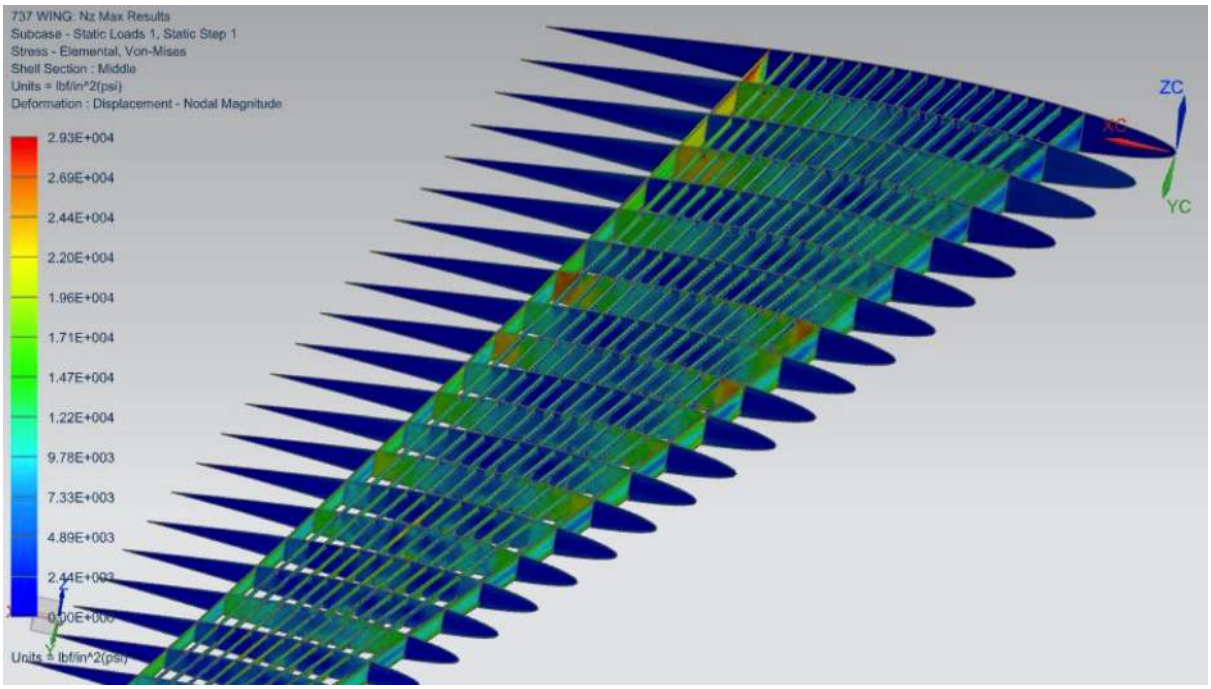

Figure 32– von Mises elemental stress surface contour of Test Case #1 wing, with wing skins hidden so that internal stresses along the spar webs, ribs, and stiffeners can be seen

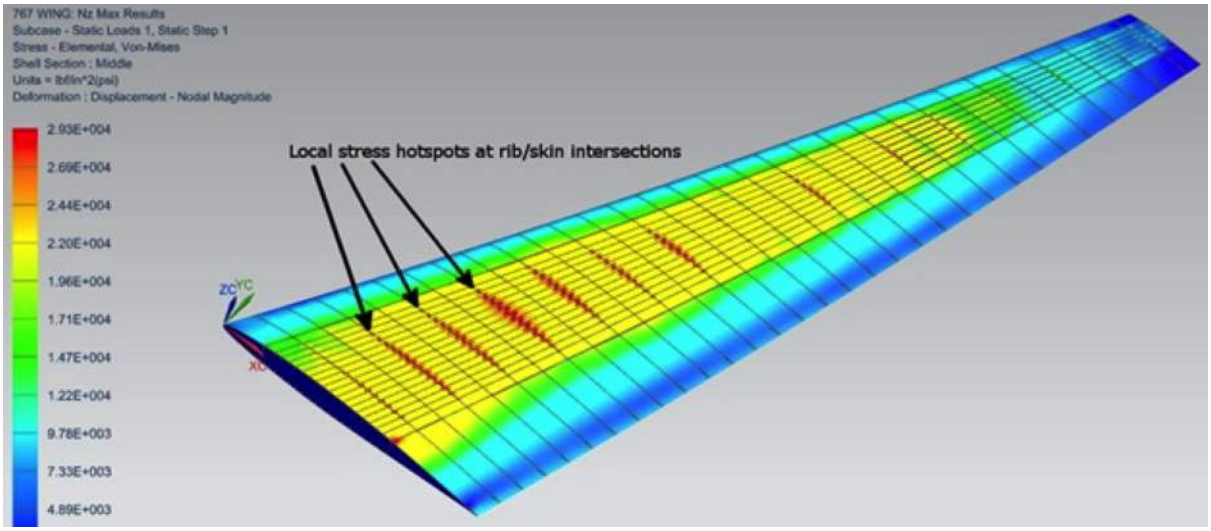

Figure 33 Local stress hotspots occurring at rib-skin intersections of the Test Case # 1wing

Local hotspots occur on the upper and lower wing skin surfaces at several of the rib-skin intersections. Higher stresses should be expected at face intersections in general because of a sharp angle of stress transfer between 2D mesh elements. However, as Figure 33 points out, some of the rib-skin intersections produce noticeably higher stresses which cannot be explained simply by face intersections. Furthermore, these local hotspots were not expecte d. The wing skins were removed and the internal structure around these hotspots was examined thoroughly. After close inspection, it was determined that these hotspots were caused by a less than ideal alignment of stiffeners between torque boxes.

When one set of stiffeners "lines up" with an adjoining set of stiffeners, the stress flow from one torque box to the next is ideal and a local hotspot is not produced. More specifically, if the chord wise distance from the stiffener-rib intersections of one torque box to the stiffener-rib intersections of the adjoining torque box on the *other* side of the rib is negilible or zero, then the stiffeners "line up". Figure 34, below, showcases this phenomenon, with the rib-skin intersection where the neighboring stiffeners don't align well being one of the locations of the stress hotspots. Additionally, notice that the forward and aft sections of the rib at this intersection are also experiencing higher stresses than the ribs with ideal stiffener alignment.

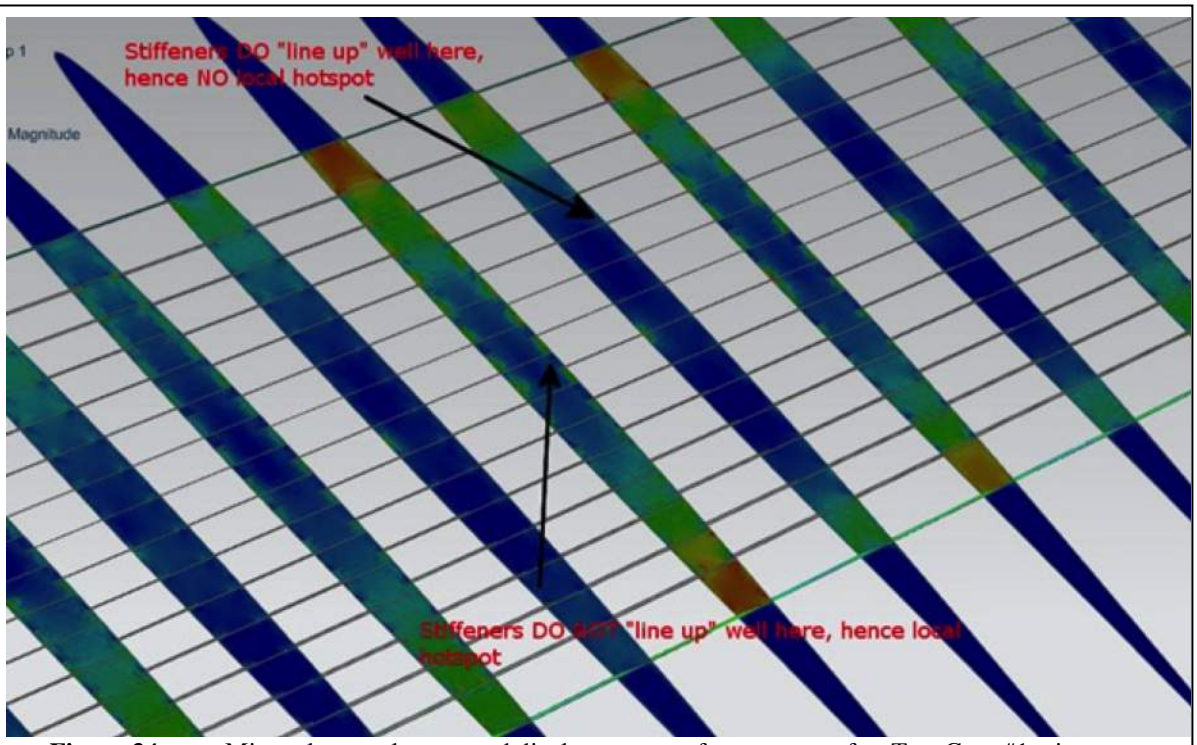

Figure 34– von Mises elemental stress and displacement surface contours for tTest Case #1 wing

IV. More Complex Validition Cases

This process from model build-up to FEM creation was repeated for two additional cases (we studied a total of four different wing geometries). In addition to the above mentioned simplified (Test Case #1) and more complex (Test Case # 2) B737 sized wings, we modelled a simplified B767 sized aircraft (Test Case #3) and a regional-jet-sized aircraft with a highly swept low aspect ratio wing (Test Case # 4). Our intention was to try significantly different geometries in order to validate the model across a wide envelope of wings.

Table 1: Summary of Validation Cases

#	Description	MTOW (lbm)	Inertial Relief	Sref (ft^2)	Wing span (ft)	Taper ratio	Aspect ratio	Quarter-chord sweep (deg.)	Thickness to Chord
1	Simple 737	116000	None	980	93	0.279	8.83	27.0	10% uniform
2	Complex Mock 737	116000	Fuel + Engine + Empirical Implied Wing Mass	980	93	0.279	8.83	27.0	14% to 10% across span
3	Simple 767	315000	None	3050	155	0.370	7.89	31.5	10% uniform
4	AR 4 RJ	100000	None	1600	80	0.350	4.00	40.0	10% uniform

Test Case # 3 comprises:

1. Maximum Take-Off Weight (315,000-lbm) used to calculate the $+Nz_{max}$ envelope load case (wingtips bend upwards)
2. Maximum Landing Weight (252,000-lbm) used to calculate the $-Nz_{min}$ envelope load case (wingtips bend downwards)
3. Design Nz_{max}=+2.5 g's
4. Design Nz_{min}=-1.0 g (flight), -2.5 g's (ground)
5. Wing Span, b=155-ft (tip-to-tip) (Structural span is 181.8-ft)
6. Wing Chord
   a. Centerline Chord, C_0 = 31.1-ft
   b. Tip Chord, C_t = 8.3-ft
7. Wing Sweep, $\Lambda_{C/2}$= 31.5°
8. Wing Area, $Sref$ = 3050-ft^2
9. Taper Ratio, TR = 0.267
10. Aspect Ratio, AR = 7.875
11. Thickness to Chord Ratio, $t/c(y)$ = 10% midspan and holding this value to the tip.
12. Distance between spars = 50% of trapezoidal planform
    a. Front Spar @ 15% chord of trapezoidal planform
    b. Rear Spar @ 65% chord of trapezoidal planform

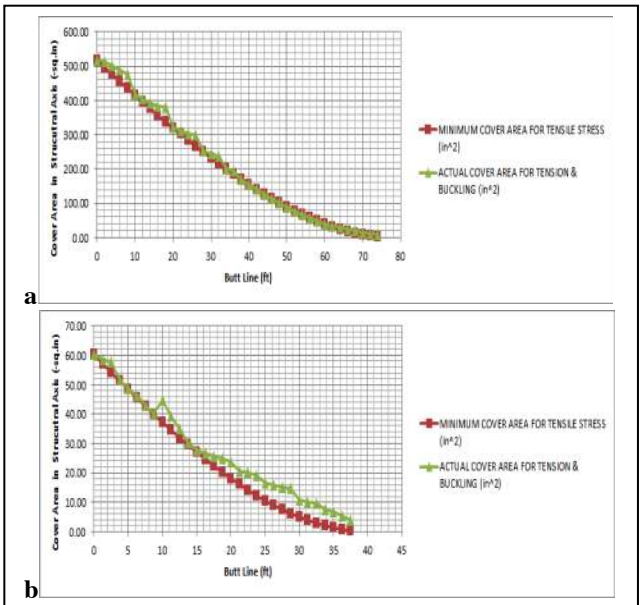

Figure 35 – Minimum Cover Area vs Actual Cover Area needed to satisfy Tension, Compression, Stiffenened Panel Buckling and Local Panel Buckling Criteria. a) Test Case # 3 b) Test Case # 4

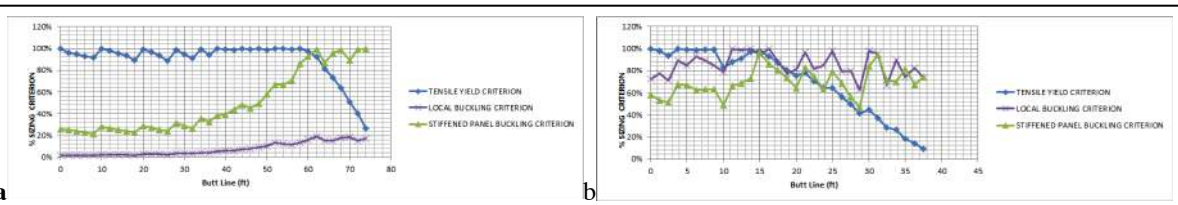

Figure 36 – sizing criteria for load sharing between spar caps, skin and stringers on optimized wing. a) Test Case #3, b) Test Case 4

13. Rib to Rib Spacing, 24-inches BL in overall aircraft coordinate frame ($\Delta y'$ = 28.2-ins in local wing reference frame)
14. Stiffener Spacing, 4-in

Test Case # 4 comprises:

1. Maximum Take-Off Weight (100,000-lbm) used to calculate the $+Nz_{max}$ envelope load case (wingtips bend upwards)
2. Maximum Landing Weight (80,000-lbm) used to calculate the $-Nz_{min}$ envelope load case (wingtips bend downwards)
3. Design Nz_{max}=+2.5 g's
4. Design Nz_{min}=-1.0 g (flight), -2.5 g's (ground)
5. Wing Span, b=80-ft (tip-to-tip) (structural span 104.4 –ft)
6. Wing Chord
    a. Centerline Chord, C_0 = 29.6-ft
    b. Tip Chord, C_t = 10.4-ft
7. Wing Sweep, $\Lambda_{C/2}$= 40°
8. Wing Area, $Sref$ = 1600-ft^2
9. Taper Ratio, TR = 0.35
10. Aspect Ratio, AR = 4.0
11. Thickness to Chord Ratio, $t/c(y)$ = 10% uniform
12. Distance between spars = 50% of trapezoidal planform
    a. Front Spar @ 15% chord of trapezoidal planform
    b. Rear Spar @ 65% chord of trapezoidal planform
13. Rib to Rib Spacing, 15-in BL in overall aircraft coordinate frame
14. Stiffener Spacing, 8-in

Referring to Figure 36a, Wing Test Case #3 is primarily sized by tensile yield criteria. With the exception of a region near the wing tips, the buckling constraints may be satisfied by redistributing area across spar caps, skins and stiffeners. Inboard the spar caps grow to a maximum allowable size in the search algorithm, 8 inches wide by 2 inches thick (referring to Figure 37a). Outboard, the structure becomes limited by the stiffened panel buckling criterion. As one moves outboard in the wing, the size of the spar caps diminishes (Figure 37a), the skin thickness declines from 0.8-in at the root to 0.15-in near the tip (Figure 38a), and the number (Figure 39a) and size (Figure 40a) of the stiffeners similarly shrinks.

The torque box of the Test Case #3 optimized wing was predicted to weigh 46,612-lbm; if sized according to tensile stress limits alone, it would weigh in at 43,917-lbm. Thus, ensuring structural stability imposes a weight penalty of 5% on this wing above that predicted by a simple bending-moment correlated wing weight equation.

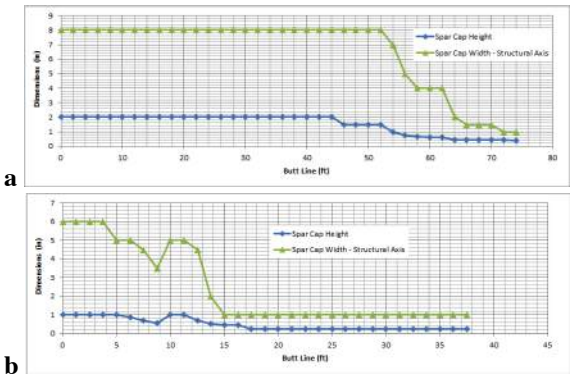

Figure 37 – Spar Cap Height & Width for alogirthm selected optimized wing. a) Test Case #3, b) Test Case 4

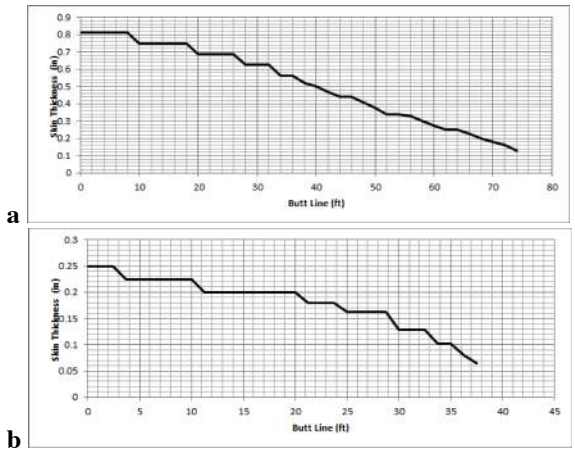

Figure 38 – Wing skin thickness (upper and lower) for optimized wing. a) Test Case #3, b) Test Case #4

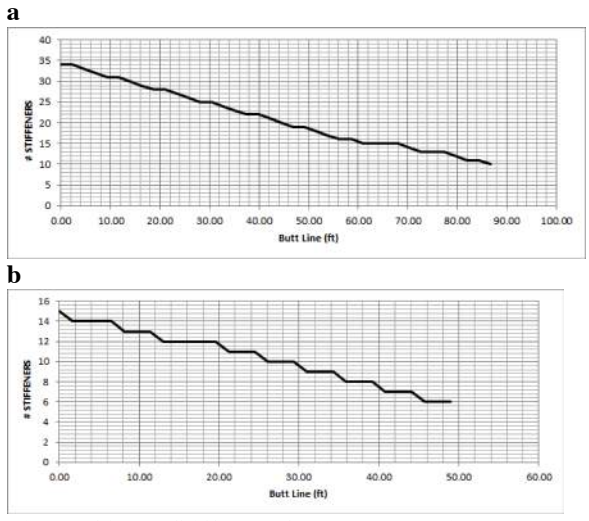

Figure 39 – # Stiffeners for upper and lower covers for optimized wing. a) Test Case # 3, b) Test Case #4

Referring to Figure 35b, Wing Test Case #4 weighs more than a simple tension based sizing approach would imply. Only the structural region near the root is sized by tensile yield criteria (See Figure 36b). Elsewhere the interplay between the buckling constraints may be satisfied by increasing the overall cross sectional area beyond that required for tension, resulting in a relative "heavy" and "stiff" wing. Where the panels are buckling dominated, the spar caps are reduced in size. They reach minimum gage of 1 inch wide by 0.25 inch thick (referring to Figure 387) by midspan. As one moves outboard in the wing, the skin thickness declines from 0.25-in at the root to 0.060-in near the tip (Figure 38b), and the number (Figure 39b) and size (Figure 40b) of the stiffeners similarly shrinks.

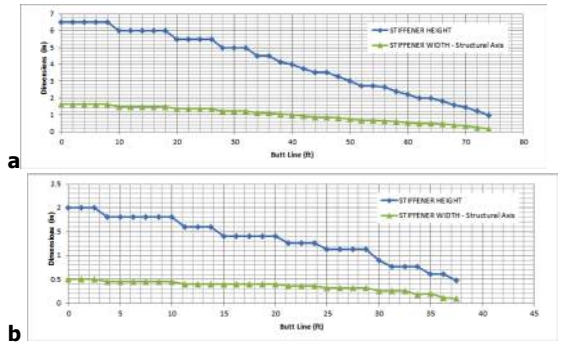

Figure 40 – Stiffener sizing per bay (upper and lower) for optimized wing. A) Test Case # 3, B) Test Case #4

The torque box of the Test Case #4 optimized wing was predicted to weigh 3374 lbm; if sized according to tensile stress limits alone, it would weight 2883 lbm). Thus, ensuring structural stability imposes a weight penalty of 17% on this wing above that predicted by a simple bending-moment correlated wing weight equation. Given the history of correlating wing structural weight to bending moments, this is a significant revelation.

D. FEM Results for Stress and Deflections

Simulation results for the *Nzmax* loading scenario for the remaining three wings are presented in this section.

In the provided elemental von Mises stress surface contours, the maximum of the contour plot was set to the maximum allowable stress dictated by the spreadsheet. The stresses plotted in the surface contours are the average/middle values between the two surfaces of the 2D shell elements. Displacement contour surface plots are also provided. As expected, maximum displacement occurs at the wing tips.

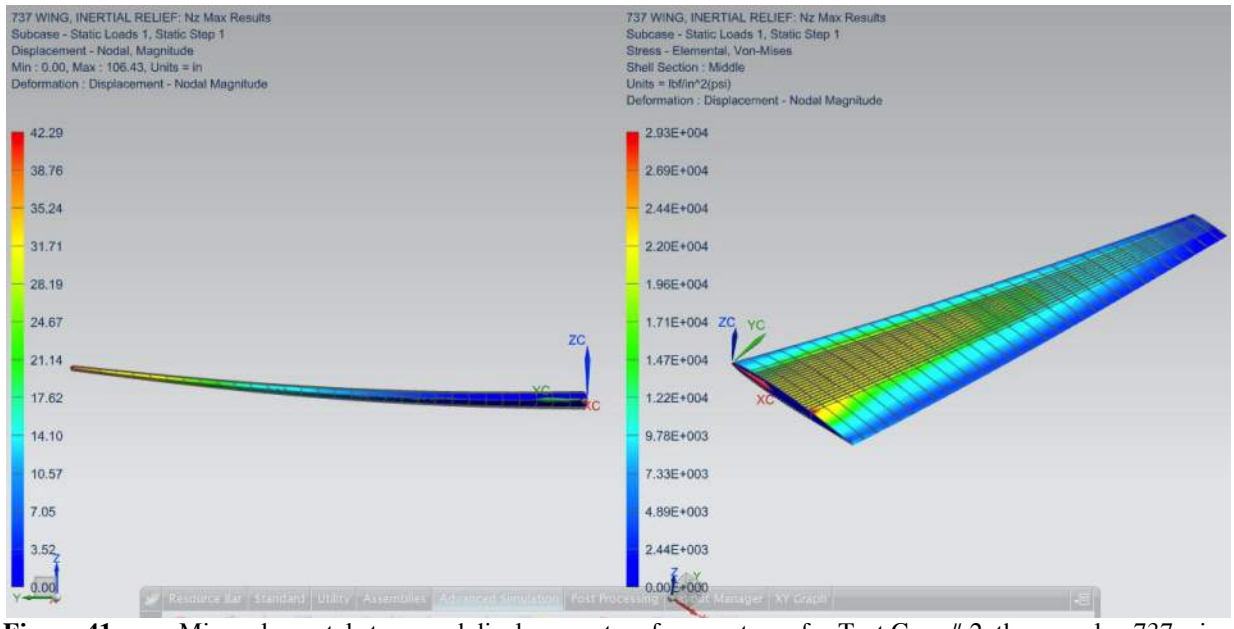

Figure 41– von Mises elemental stress and displacement surface contours for Test Case # 2 the complex 737 wing

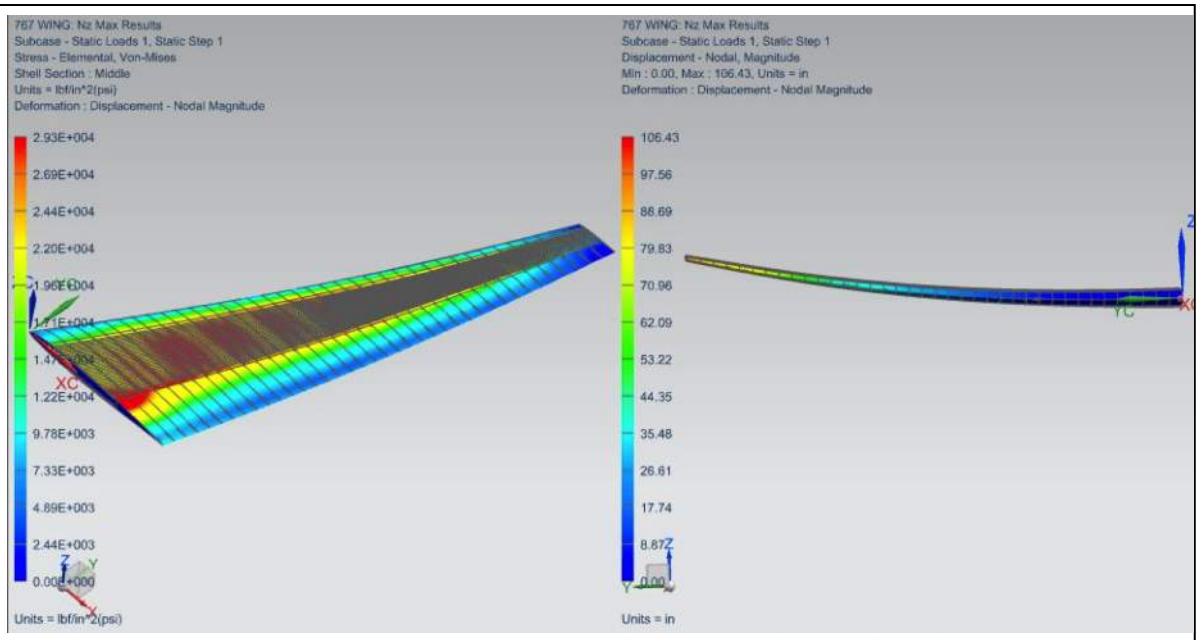

Figure 42– von Mises elemental stress and displacement surface contours for Test Case #3, the mock 767 wing

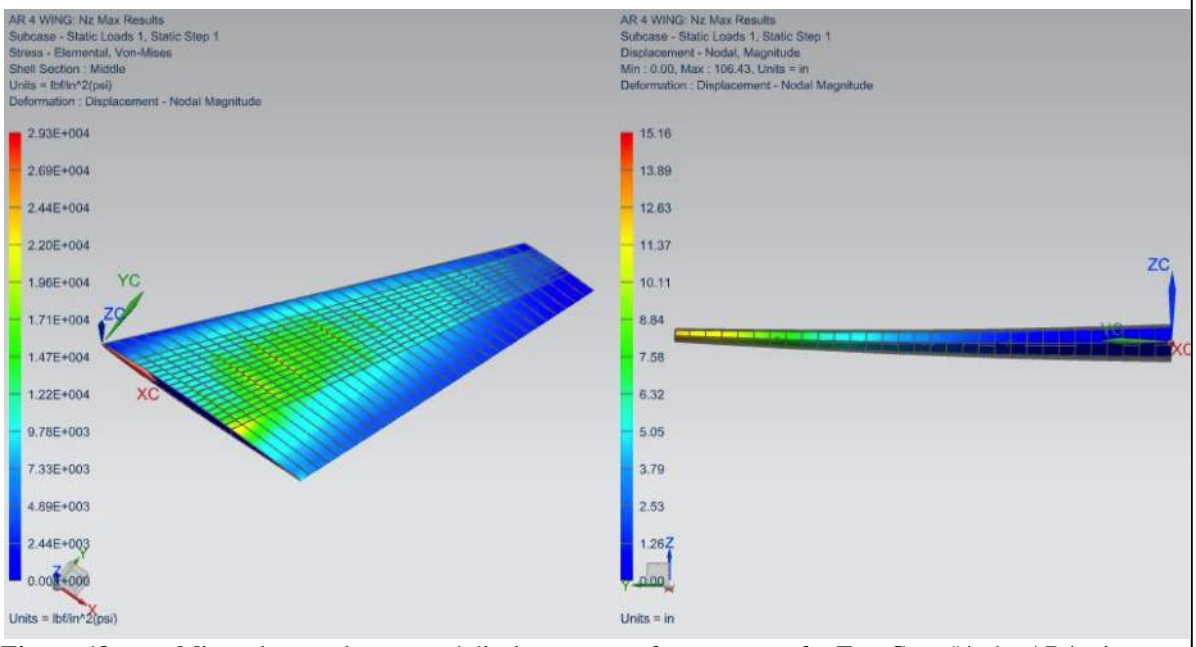

Figure 43– von Mises elemental stress and displacement surface contours for Test Case #4, the AR4 wing

As a result of being buckling, rather than stress dominated, the low aspect ratio wing (Test Case #4) obviously experienced the mildest stresses and least displacement at the wing tips. While the majority of the mock 767 wing experienced stresses below the maximum set by the spreadsheet, that wing geometry had the most intense and numerous stress hotspots. The mock 737 wing performed the "best" of the three wing geometries. Remember that the spreadsheet attempts to size the wing so that weight is optimized meaning that high loading is expected but not to a magnitude that exceeds the limit defined by the designer. The trapezoidal 737 wing achieved high stresses over the majority of the surface area but with less than 10 hotspots among its entire geometry, resulting in what can be deemed as an optimized structure.

E. FEM Weights vs. Analytical Torque Box Weights

A new version of the fully-defined sheet body aircraft wing is exported and saved to be used to calculate the mass properties of the torque box. All the sheet bodies that compose the torque box are thickened into solid bodies according to the thicknesses specified by the spreadsheet. The thickness is applied symmetrically to the sheet bodies in the two directions normal to the sheet body.

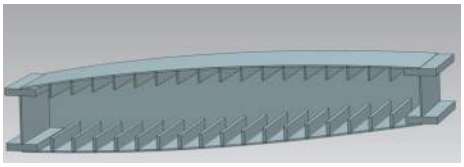

Figure 44 Areas of overlap can be seen at the intesections of solid bodies, namely at the stiffener-skin intersections

In order to ensure an accurate calculation of mass properties, Boolean operations must be used. When two intersecting sheet bodies are thickened there is an area of overlapping solid bodies. If you do not alleviate this issue and assign density properties to the solid bodies, *NX* will "double count" the mass in these overlapping areas, resulting in an exaggerated weight of the torque box. The solid bodies were united via Boolean operations in the following order: stiffeners to skins, ribs to skins, spar web to spar caps, and finally spar caps to skins.

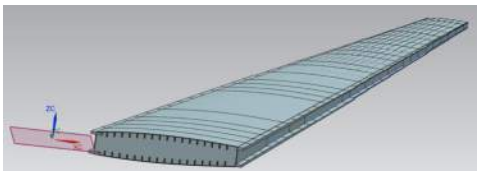

Figure 45 Full span of mock 737 wing torque box

This order was a strategic choice. Remember that when two solid bodies are united they operate as a single solid body. Suppose it was chosen to unite the ribs to skins and then the spar webs to skins before the stiffeners. This would then make it impossible to hide the ribs and spar web in order to view the interior of the wing and select the stiffeners without also hiding the skins. In summary, it is imperative to unite the most interior components first to the skins and then progressively work your way to the most exterior components. The CAD and FEM reported structural masses differed from the spreadsheet calculated mass by approximately 2.8%.

The mass of the solid model of the mock 737 wing is remarkably close to its thoeretical value calculated by the spreadsheet. This slight but acceptable deviation is likely due to the way the spar caps are thickened. Ideally, they would be thicken in the chordwise direction. However, the *Thicken* comamand in *NX* does not allow for anything but thickening in the direction normal to the sheet body. Of course, the model could have been built in a manner to perfectly match the mass set by the spreadsheet but instead the main intention was to build a model of sheet bodies for use with 2D shell meshing.

V. System Design Level Trade Studies

Because our system seems to design rational, physically plausible wings that meet certification requirements, we can use this tool in a statistical design manner. We can explore the effects of changing detail design parameters as well as aircraft configuration aerodynamics parameters on wing weight. Returning to the simplified B737 type geometry of Test Case #1, we can run a few, simple trade studies. More complex trade studies will be found in a subsequent manuscript to be published later in 2015.

Figures 46 and 47 are the results of a trade study examining the effect of stiffener spacing and inter-rib spacing upon wing weight.

From a perspective of predictive capability using the more complex tension and buckling model for wing weight (Figure 46), as the rib-to-rib spacing increases from 12-inches to 24-inches the amount of additional structural weight to ensure local and overall stiffened panel stability increases. For the narrowest studied rib spacing, actual wing weights run around 10% above that predicted by the tension criterion alone. For the larger rib spacings, actual wing weights run as high as 40% above that predicted by the tension criterion.

From the viewpoint of a simplified-tension-only basis for total wing weight (Figure 47), there is a clear “optimum” rib-to-rib spacing found around 18-inches. Below and above that spacing, total wing weight increases; as the rib-to-rib spacing decreases, the weight of the increasing number of ribs themselves begins to adversely impact

wing weight. At the same time, the overall wing weight isn't terribly critical in terms of the small changes in the stiffener spacing arrangement (although the details of the sizes of the individual stiffeners change as the spacing is altered – one can achieve adequate overall stiffened-panel buckling will have fewer, larger or more more numerous, smaller stiffeners).

What is fascinating is the observation that the "system level" optimal design (that of minimum structural mass) is found where a significant portion of the wing is sized by buckling rather than basic tensile strength constraints.

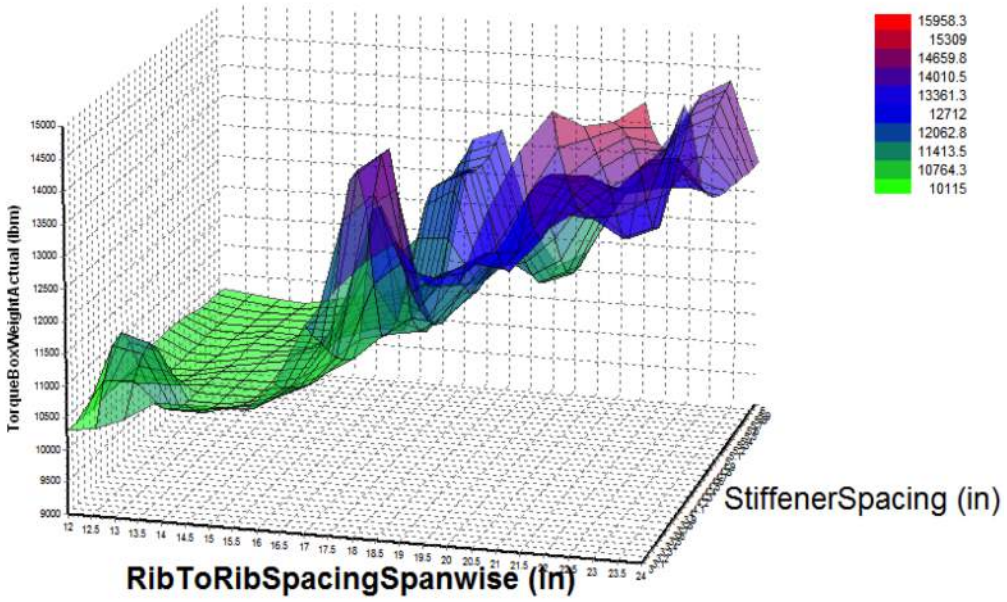

Figure 46–- Effective of inter-rib (span wise) and stiffener (chord wise) spacing on optimized wing weight (holding MTOW, MLW, Nzmax, Nzmin, planform area, sweep, span, and t/c distribution constant)

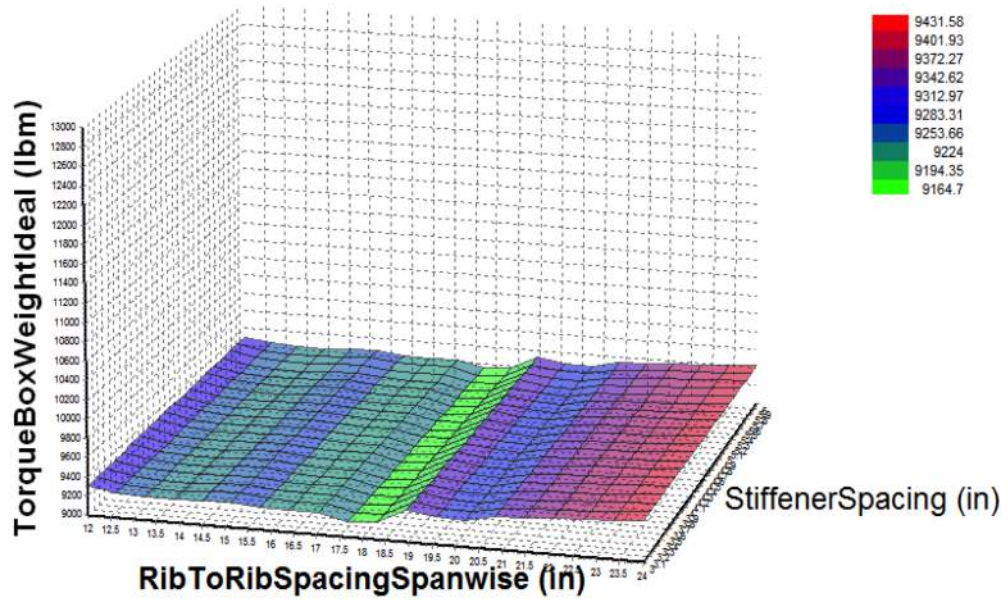

Figure 47–- Effective of inter-rib (span wise) and stiffener (chord wise) spacing on the idealized tension structure wing weight (holding MTOW, MLW, Nzmax, Nzmin, planform area, sweep, span, and t/c distribution constant)

VI. Conclusions

All four wing geometries did have the same type of hotspots occur at certain rib-skin intersections, albeit at varying degrees of severity and number. It was found when examining the internal structure that this is due to how similar a set of adjacent stiffener patterns are to each other. More specifically, if a set of stiffeners "line up" with an adjacent set at their shared rib then they more effectively carry loads across the torque box intersection. However, when there is significant chordwise distance between one stiffener and an adjoining one then stress concentrations arise and result in the local hotspots seen on the upper and lower wing skins (refer back to Figures 33 and 34 for visual clarification of this structural phenomenon). In a final design, engineers should make the effort to "line up" as many adjoining stiffener sets as possible instead of evenly spacing them chordwise along the torque box.

In summary:

1. The majority of the mock 737 wing generated with inertial relief involved produced stresses under the allowable limit for the *Nzmax* scenario. However, the most inboard spar web panel did have significant amounts of its 2D elements experience stresses above this limit, with the average exceeding stress being about 110% of the allowable value.
2. The optimizer designed mock-767 wing (Test Case #3) may be operationally found to be potentially overly flexible (though certainly it is strong enough from a static perspective). Its weight was fairly close (5% over) that predicted using only a bending-moment / tensile-stregth estimation method.
3. The optimizer designed low aspect ratio wing (Test Case #4) could be considered overly stiff and heavier than anticipated from a simple tensile force model. The stiffness and weight came with good reason as the structural sizing was governed by buckling rather than tensile stress cases. The practical wing was 17% heavier than that predicted using a bending-moment / tensile-stregth estimation method.

Acknowledgments

This manuscript derives from work Mr. Lemonds performed in partial fulfillment of the degree requirements for obtaining his M.S. in Aerospace Engineering from Arizona State University. All analysis on this unfunded project was completed at Arizona State University.

References

[1] Raymer, D. *Aircraft Design : A Conceptual Approach*, AIAA, 2006.
[2] Roskam, J., Airplane Design. Part V. Component Weight Estimation, DAR Corp, 1999.
[3] Nicolai, L., *Fundamentals of Aircraft Design*, METS, 1974.
[4] Torenbeek, E., "Prediction of Group Weight for Preliminary Design," Aircraft Engineering, pp. 16-21. July 1971.
[5] Torenbeek, E., *Synthesis of Subsonic Airplane Design*, Delft University Press, Delft, Holland, 1982
[6] McCullers, L.A., FLOPS: Aircraft Configuration Optimization. NASA CP-2327, 1984
[7] Norton, W. "Lockheed C-5 Galaxy – Warbird Tech Vol 36," Speciality Press, 2003.
[8] Niu, M.C.Y., *Airframe Structural Design*, 2nd Ed, Hong Kong Conmilit Press Ltd, 1988.
[9] Niu, M.C.Y., *Airframe Stress Analysis and Sizing*, 2nd Ed. Hong Kong Conmilit Press Ltd., 1997.
[10] 14 CFR § 25.337 (2014). *Limit maneuvering load factors*. ("Except where limited by maximum (static) lift coefficients, the airplane is assumed to be subjected to symmetrical maneuvers resulting in the limit maneuvering load factors prescribed in this section. … The positive limit maneuvering load factor *n* … may not be less than 2.1+24,000/(W+10,000) except that *n* may not be less than 2.5 and need not be greater than … The negative limit maneuvering load factor … may not be less than −1.0")
[11] MIL HDBK 5-J
[12] 14 CFR § 25.303 (2014). *Factor of safety*. ("Unless otherwise specified, a factor of safety of 1.5 must be applied to the prescribed limit load which are considered external loads on the structure.")
[13] Capone, F.J. "Wind Tunnel/Flight Data Correlation for the Boeing 737-100 Transport Airplane," NASA TM X-72715, August 1975.
[14] Boeing, *Jet Transport Performance Methods*, Flight Operations Enginereing, D6-1420, 7th Ed., May 1989.
[15] MSC Software. *Linear Static Analysis User's Guide: MSC Nastran 2012*, MSC Software, 2011.